



# Capacitance-Based Levelmeter Read-Out for the Münster Dual Phase Xenon Time Projection Chamber

Bachelor thesis

Denny Schulte

Westfälische Wilhelms- Universität Münster

Institut für Kernphysik

AG Prof. Dr. C. Weinheimer

2016

Referent: Prof. Dr. C. Weinheimer

Korreferent: PD Dr. C. Klein-Bösing

# Contents

<b>1</b>	<b>Introduction</b>	<b>1</b>
<b>2</b>	<b>The Münster TPC</b>	<b>3</b>
2.1	Design and Functionality . . . . .	3
2.2	Design and Read-Out System of the Levelmeters . . . . .	6
<b>3</b>	<b>Design and Test of a LabVIEW-Based Slow Control</b>	<b>11</b>
3.1	LabVIEW . . . . .	11
3.2	Building of a Custom Made Driver for the Levelmeter Read-Out . . . . .	12
3.3	Capacitance Measurement of a Levelmeter with the Custom Made Driver in Liquid Nitrogen . . . . .	16
3.4	Levelmeter Read-Out Set-Up for the Münster TPC . . . . .	20
<b>4</b>	<b>Capacitance Measurements of the Münster TPC Levelmeters</b>	<b>25</b>
4.1	Calibration of the Levelmeters during Filling and Recuperation . . . . .	25
4.2	Stability of Liquid Level during Operation . . . . .	32
<b>5</b>	<b>Conclusion and Outlook</b>	<b>36</b>
<b>6</b>	<b>Appendix</b>	<b>38</b>
<b>7</b>	<b>Bibliography</b>	<b>45</b>

# 1 Introduction

For a considerable time, the composition of the universe has been an unresolved problem for astrophysicists due to the fact that the whole universe mostly consists of widely unknown components called dark energy and dark matter. Meanwhile there are a few collaborations to find out the characteristics and compound of this dark mystery. At least, according to present-day research, dark matter is believed to be stable, non-baryonic, non-electromagnetic, cold meaning non-relativistic as well as massive and to have a cross-section on the scale of the weak interaction. A currently most hopeful particle candidate for this dark matter which fulfills all of these attributes is the Weakly Interacting Massive Particle (WIMP).

One of the collaborations, the XENON Dark Matter Project, searches for the WIMP and uses, in order to detect this particle, a dual-phase Time Projection Chamber (TPC) filled with pure xenon and is geared towards scattering of WIMPs with xenon nuclei. This method leads to the advantage of producing a three-dimensional position reconstruction of each event because two signals can be measured, one direct scintillation signal in the liquid phase of the xenon and one charge signal in the gaseous. Xenon is expedient as a detector material because of the high atomic number and density with a great radioactive self-shielding and a big scattering cross-section.

There are three stages of the Xenon Dark Matter Project constructed in the Laboratori Nazionali del Gran Sasso (LNGS) in Italy at a depth of about 3600 m water equivalence so far: XENON10, XENON100 and XENON1T.

The XENON10 project, established in 2006, achieved with a detector volume of 15 kg xenon the best sensitivity for the scattering of a WIMP and a xenon nucleus at that time [Ang08]. The next stage of this collaboration, XENON100, has a fiducial xenon volume of 62 kg and a sensitivity of  $\sigma_{SI} = 2 \cdot 10^{-45} \text{cm}^2$  for a 55 GeV WIMP. After 225 days of measurement no evidence for the WIMP could still be found [Apr12a]. By means of bigger dimensions of the experiment and further improvements the current generation, XENON1T, obtains a spin-independent, two more order of magnitude sensitivity of  $\sigma_{SI} = 2 \cdot 10^{-47} \text{cm}^2$  for a 50 GeV WIMP [Apr12b].

In order to realize and test new technologies, the Münster Xenon Group has built its own TPC with smaller dimensions. Therefore, it is possible to make both internal and external calibration and data analysis.

This thesis aims at making a capacitance-based levelmeter read-out for the Münster Dual Phase Xenon Time Projection Chamber. To this end, the Münster TPC has three levelmeters on hand which monitor the liquid level of the xenon in the liquid phase. In addition to this, a search for an option to switch between the levelmeters and readout the data was needed.

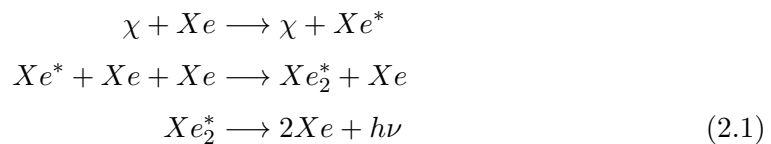
At first, there will be a presentation of the design and functionality of the Münster TPC, which will be followed by an introduction of LabVIEW. Afterwards, the design and test of a labview-based slow control will be explained. Furthermore, capacitance measurements with the calibration of the levelmeters and stability of the liquid level will be shown. A conclusion as well as an outlook will finally sum up the results of this thesis and point further research out.

## 2 The Münster TPC

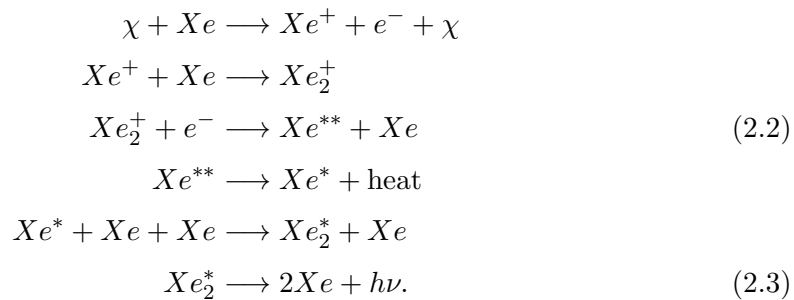
This chapter includes a presentation of the Münster TPC. At first, the design and functionality will be discussed, followed by a detailed presentation of the implemented levelmeters.

### 2.1 Design and Functionality

In 2011 the Münster Xenon Group has built an own TPC (fig. 2.1). The cylindrical detector with a height of 334 mm and an external diameter of 155 mm has a total volume of about 2.56 kg xenon. This xenon volume consists of liquid xenon with a small gaseous phase above. The bottom as well as the top of the detector is equipped with seven photomultiplier tubes (PMTs) by Hamamatsu Photonics<sup>®</sup>. The inner volume is surrounded by polytetrafluorethylen (PTFE) blocks, due to the fact that PTFE has a high efficiency to reflect xenon scintillation light and can be produced with high purity in term of radiation. These blocks are encompassed by another stainless steel tube, the cryostat. In order to prevent thermal losses, the cryostat is housed in a stainless steel vacuum chamber. The interaction of some particles  $\chi$  with xenon nuclei  $Xe$  leads to both an excitation[Apr09]:



and an ionization of the nuclei[Apr09]:



During the process of excitation, a direct vacuum ultraviolet scintillation light of 178 nm follows due to the excited xenon forming an excimer with another xenon nucleus which relaxes into the ground state by radiation (eq. 2.1). As a consequence, xenon is transparent for its own scintillation light, allowing the PMTs at the top and the bottom to detect the produced light. In addition, the ionization process causes an excited xenon nucleus (eq. 2.3). These two prompt scintillation signals can be detected by the PMTs called signal S1. The resulting electron-ion pairs of the ionization are separated by an electric field. For this purpose, an applied cathode mesh on the bottom of the detector with a potential of up to  $-17$  kV and 12 regular distanced copper field shaping rings between the cathode mesh and the grounded gate mesh ensure a homogeneous drift field of about 1 kV/cm. A stronger electric field with up to 10 kV/cm extracts the electrons into the gaseous phase, and therefore they gain enough energy to produce a second light of scintillation called S2 (eq. 2.2). Due to the constant electric field, the z-position of any event can be calculated by the electron drift time. Considering that the x- and y-coordinate is determined by the array of the PMTs at the top, a 3D position reconstruction of each event can be achieved.

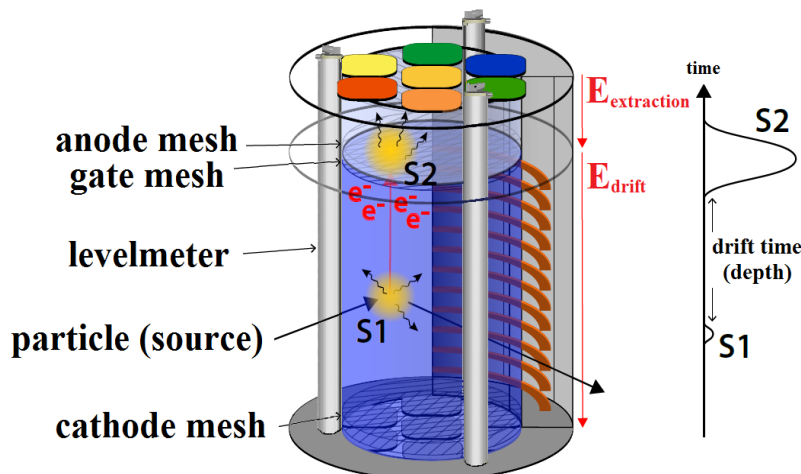


Figure 2.1: Schematic construction and working principle of the Münster TPC. The photomultiplier tubes can detect two signals: The prompt scintillation light (S1) and a ionisation signal (S2). The depth of the interaction point can be obtained by the time difference between the two signals. In addition, the x- and y-position can be determined by the array of PMTs at the top, leading to a 3D position reconstruction. Drawing by Lutz Althüser.

This 3D position reconstruction leads to the opportunity of event discrimination because just events of a fiducial volume in the middle of the detector have enough background self-shielding by the surrounded xenon to be not any background particle. Another important point of discrimination, just nuclear recoils are qualified for dark matter, because of the requirement of a non-electromagnetic interacting particle (chap. 1). For this reason, one has to differentiate between electronic and nuclear recoils. Electronic recoils occur at beta or gamma rays. Due to less ionization of nuclear recoils, the S2 is smaller (fig. 2.2).

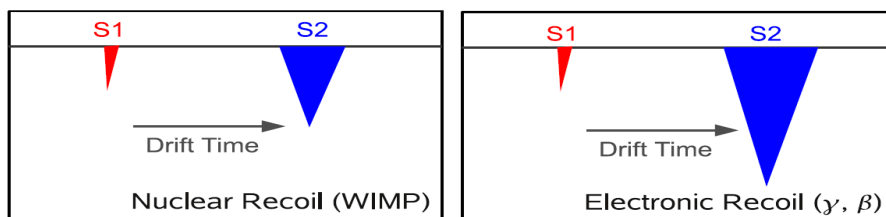


Figure 2.2: Sketch of the waveforms of two type of events. The different ratio of the charge (S2) and the light (S1) signal allows for the discrimination between nuclear recoils from WIMPs and neutrons and electronic recoils from gamma- and beta-background [Apr12c].

Thus, an event can be identified as nuclear recoil if the S2 to S1 ratio is small. Whereas a big ratio results out of an electronic recoil. In order to get a meaningful S2 to S1 ratio, the PMTs have to be calibrated. Therefore a glass fiber for LED gain calibrations have been recently integrated (further information of gain calibration shown in [Bla15]). In addition, the level of the liquid xenon phase could influence the ratio. Due to the fact that the difference between grounded gate mesh and anode mesh is just 5 mm, the liquid xenon level need to be kept stable at the level of the gate mesh in order that preferably many electrons can be extracted in the gaseous phase. For this purpose, three capacitance-based levelmeters with a height of 294 mm have been implemented, in order to monitor the liquid xenon level. The development of a new read-out of these meters is presented in the next section.

## 2.2 Design and Read-Out System of the Levelmeters

The three integrated levelmeters with a length  $l$  of 294 mm are composed of 6 mm steel tubes with an inner diameter of 4 mm ( $D$ ) and 3 mm steel rods ( $d$ ) (fig. 2.3). The steel tube has a 1 mm slit to prevent capillary effects. In addition, tube and rod are isolated from each other by a polyether ether ketone spacer and function as capacitor plates of a cylindrical capacitor. Due to the fact that there is a difference between the dielectric constants of the liquid xenon and the xenon gas ( $\Delta\epsilon_r$ ) the capacitance between the rod and the tube depends on the filling level of liquid xenon.

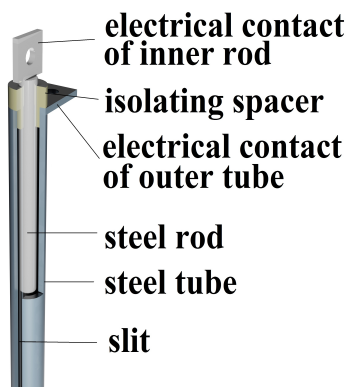


Figure 2.3: CAD drawing of one levelmeter of the Münster TPC. The liquid xenon level of the Münster TPC can be monitored by a cylindrical capacitor. The capacitor plates are isolated from each other by insulating spacers. Besides, a 1 mm slit in the outer tube prevents capillary effects. Drawing by Christian Huhmann.

In order to measure the capacitance of a cylindrical capacitor, a potential difference  $U$  has to be applied between the cylindrical plates. According to this, the capacitance  $C$  results from

$$C = Q/U, \quad (2.4)$$

with the saved electric charge  $Q$  between the plates. The electric field between the cylindrical plates decreases radial. Due to the fact that the electric field intensity  $E$  at every point is identically equal to the voltage gradient of that point, equation 2.4 is rewritten to

$$C = \frac{Q}{\int \vec{E}(\vec{r})d\vec{r}} = \frac{Q}{\int_d^D \frac{Q}{2\pi l \epsilon_0 \epsilon_r \cdot r} dr} = 2\pi l \epsilon_0 \epsilon_r \cdot \frac{1}{\ln(D/d)}. \quad (2.5)$$

Incidentally the Gauss' theorem is used.  $\epsilon_0 = 8.854187817 \cdot 10^{-12}$  F/m is the vacuum permittivity [Lid09] and  $\epsilon_r$  the relative permittivity of the medium between the plates. Hence the levelmeters measure the liquid level between liquid and gas, equation 2.5 will be extended. A certain liquid level can be understood as two parallel placed levelmeters, one in the liquid and one in the gaseous phase. Thus the whole capacitance results from the sum of these. If the liquid filled levelmeter has a total height of  $l_1$  and the meter of the gaseous phase a height of  $l - l_1$ , the whole capacitance is calculated by

$$\begin{aligned} C &= 2\pi l_1 \epsilon_0 \epsilon_{r_L} \cdot \frac{1}{\ln(D/d)} + 2\pi(l - l_1) \epsilon_0 \epsilon_{r_G} \cdot \frac{1}{\ln(D/d)} \\ &= 2\pi l_1 \epsilon_0 \Delta \epsilon_r \cdot \frac{1}{\ln(D/d)} + 2\pi l \epsilon_0 \epsilon_{r_G} \cdot \frac{1}{\ln(D/d)}. \end{aligned} \quad (2.6)$$

$\Delta \epsilon_r$  is the difference between the relative permittivity of liquid and gaseous ( $\epsilon_{r_L} - \epsilon_{r_G}$ ). The second summand of equation 2.6 gives the constant capacitance for a levelmeter fulfilled just with gas and therefore, the change in capacitance  $\Delta C$  of a cylindrical, capacitance-based levelmeter at filling or emptying with liquid is dependent upon the filling height  $l_1$  of liquid:

$$\Delta C = 2\pi l_1 \epsilon_0 \Delta \epsilon_r \cdot \frac{1}{\ln(D/d)}. \quad (2.7)$$

Consequently, using equation 2.7 the change in capacitance per millimeter change in liquid level of a xenon filled levelmeter with above-mentioned dimensions can be obtained:

$$\frac{\Delta C_{Xe}}{mm} = 2\pi\epsilon_0 \cdot \frac{\Delta\epsilon_{r_{Xe}}}{\ln(4/3)} = (0.170 \pm 0.024) \text{ pF/mm}, \quad (2.8)$$

calculated with a difference between the dielectric constants of  $\Delta\epsilon_{r_{Xe}} = 0.878$  [Lid09] and the error propagation

$$\Delta\left(\frac{\Delta C_{Xe}}{mm}\right) = \sqrt{\left(-2\pi\epsilon_0 \frac{\Delta\epsilon_{r_{Xe}}}{D \cdot (\ln(D/d))^2} \Delta D\right)^2 + \left(2\pi\epsilon_0 \frac{\Delta\epsilon_{r_{Xe}}}{d \cdot (\ln(D/d))^2} \Delta d\right)^2}.$$

The capacitor diameters are measured with a measuring inaccuracy of 0.1 mm. The other parameters were assumed as constant because the inaccuracy was unknown.

Taking this into account, the total capacitance for a fully filled cylinder is expected to be

$$C_{max} = 2\pi\epsilon_0 \cdot \frac{0.878 \cdot 0.294}{\ln(4/3)} = (49.918 \pm 0.072) \text{ pF}, \quad (2.9)$$

with the error propagation

$$\Delta C_{max} = \sqrt{\left(\frac{-2\pi l \epsilon_0 \Delta\epsilon_{r_{Xe}}}{D \cdot (\ln(D/d))^2} \Delta D\right)^2 + \left(\frac{2\pi l \epsilon_0 \Delta\epsilon_{r_{Xe}}}{d \cdot (\ln(D/d))^2} \Delta d\right)^2}.$$

For testing the newly developed read-out system as described in chapter 3.3, a slightly different levelmeter based on the same design was tested outside the TPC in a liquid nitrogen environment. With an inner tube diameter of  $D = 10$  mm, an outer rod diameter of  $d = 9$  mm and a relative permittivity difference for gaseous and liquid nitrogen  $\Delta\epsilon_{r_N} = 0.467$  [Lid09], the expected change in capacitance per mm can be computed using again equation 2.7 and the error propagation for the capacitance change per millimeters as aforementioned:

$$\frac{\Delta C_N}{mm} = 2\pi\epsilon_0 \cdot \frac{\Delta\epsilon_{r_N}}{\ln(10/9)} = (0.247 \pm 0.035) \text{ pF/mm}. \quad (2.10)$$

The theoretically calculated values (eq. 2.8, eq. 2.9 and eq. 2.10) can be compared later on in chapter 3.3 with the levelmeter read-out in liquid nitrogen and in chapter 4.1 with the measurement of the TPC levelmeter read-out in the liquid xenon reservoir. In order to measure the levelmeter capacitances inside the TPC, a newly custom-made hardware set-up was needed and is presented in the following. A basic scheme can be seen in figure 2.4.

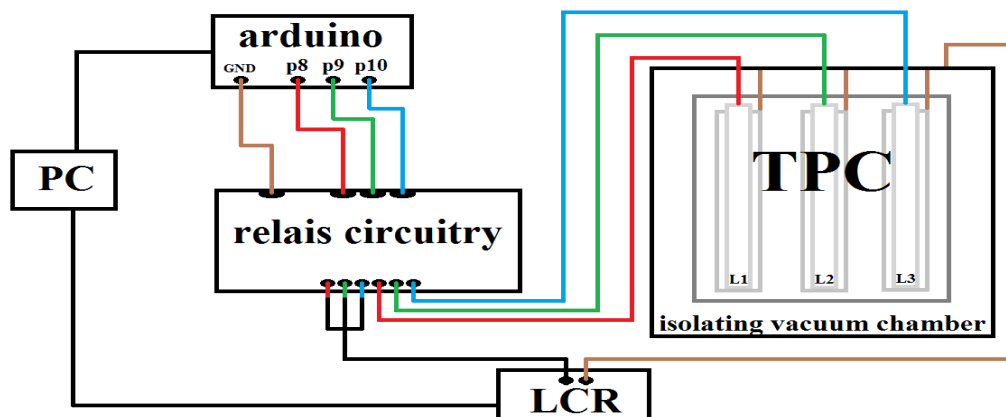


Figure 2.4: Schematic of the Münster TPC levelmeter read-out hardware set-up. A LCR-meter is used for the capacitance measurement. In order to switch between the three implemented levelmeters of the TPC, an arduino board in combination with a relais circuitry is used.

As seen in figure 2.4, the levelmeters of the TPC have two connections each. One connection, the common ground, is connected with a LCR. A LCR-meter is an electronic device to measure inductance (L), capacitance (C) and resistance (R). In this case, the LCR-meter need to measure the capacitance of the levelmeters. Due to expected capacitances in scale of picofarad the LCR-meter has to be potential-free. A non-potential-free LCR is tried out by Julian Blanke with the result that the measured capacitance values fluctuate of about several hundreds of picofarad [Bla15]. For the purpose of measuring capacitances, the LCR-meter sends a voltage with a predefined frequency and the required potential difference as aforementioned is applied.

For the Münster TPC levelmeter read-out hardware set-up, a customary handheld LCR-meter, the Agilent<sup>®</sup> U1732C with a few functions of data analysis, is used. According to the characteristics of 20000 counts resolution, a basic accuracy of 0.2 % and four different test frequencies the LCR-meter fulfills the demand of the capacitance-based levelmeter

measurement [Key15]. The device accuracy for capacitance specifications in a range of hundreds of pF and with a test frequency of 1 kHz is given as  $\pm 0.5\%$  of the reading capacitance value at a temperature of  $(23 \pm 5)^\circ\text{C}$  with a relative humidity less than 80% [Key14]. This means, the measured capacitance value can differentiate from the true capacitance by 0.5%. In addition, the manufacturer Keysight Technologies guarantees a resolution of 0.1 pF between measured capacitances of 200 pF up to 2000 pF [Key14]. The resolution is the smallest change, which can be appreciated by the device. These specifications are needed later on at capacitance measurements and stability tests.

Returning to the read-out hardware set-up in figure 2.4, the second connection of the levelmeters goes to a relais circuitry. Combined with an arduino board, the circuitry affords an opportunity to switch between the three levelmeters which is presented detailed in chapter 3.4. In order to operate with the switching system and submit data of the LCR-meter measurements to computer, the system design software LabVIEW is used which will be presented in the next chapter.

## 3 Design and Test of a LabVIEW-Based Slow Control

This chapter shows an introduction of the system design software LabVIEW, as well as the building of a custom made driver to operate with the LCR-meter. In addition, first measurements of a liquid nitrogen level will be presented, ending with a description of the switching set-up for the operation of three levelmeters and the final slow control program.

### 3.1 LabVIEW

Laboratory Virtual Instrumentation Engineering Workbench (LabVIEW) is a system design software with a graphical programming syntax by National Instruments<sup>®</sup>. The flexible concept is that the hardware is reproduced virtually to the computer. In the present-day research it is applied to facilitate data acquisition, monitoring and controlling of many devices. The dataflow programming language is called "G". LabVIEW programs or subprograms are named virtual instruments (VIs). The advantage of LabVIEW is that each VI can either stand alone or be included in another as a sub-VI. A LabVIEW-program is composed of a front panel and a block diagram. The front panel uses input variables, called controls, and output variables, called indicators, showing up on the block panel as terminal blocks which can be connected with function blocks by using wires. Therefore, the graphical code is located on the block panel and the user interface is shown on the front panel. More information about LabVIEW can be found in [Nat16a]. This system design software can be used to build a driver for operation with the LCR-meter which will be presented in the following.

## 3.2 Building of a Custom Made Driver for the Levelmeter Read-Out

As mentioned in the last chapter, the capacitances of the levelmeters are measured with the Agilent U1732C handheld LCR-meter. This device operates with Standard Commands for Programmable Instruments (SCPI) which are used to query the meter and set different read-out modes. For this purpose, LabVIEW provides an opportunity to use the standard commands for operation. Due to the fact that no library exists for the used agilent device, a new VI is required. Hence, a custom made driver of LabVIEW is programmed for sending commands and receiving answers. The LabVIEW-based Virtual Instrument Software Architecture (VISA) was used to supply the interface between LabVIEW and the USB junction. In addition, LabVIEW contains a VISA package composed of VISA Express-VIs to operate with devices. Subsequently, the first LabVIEW-based query of the LCR-meter was created with suggestions of [Geo15].

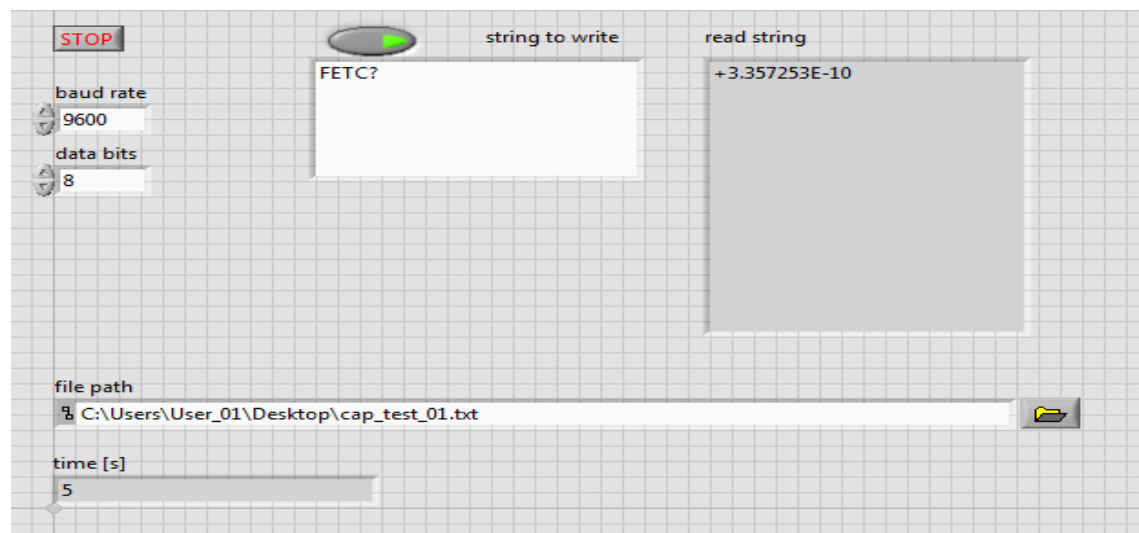
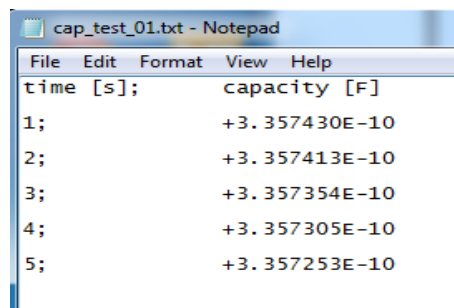


Figure 3.1: Front panel of the custom made driver. The different configurations of the LCR-meter, the file path and the SCPI both of setting and querying can be set up.

The front panel (fig. 3.1) displays controls of the serial port configuration, including the *Baud Rate* and the *Data Bits*. These configuration settings are variable in the custom made driver and need to be taken from the handbook of the LCR-meter. The *Baud Rate* is the symbol rate in symbols per second and the factory setting of the

LCR-meter is 9600. Consequently in a digital system with a binary code, a baud rate of 9600 equals to 9600 bits per second. *Data Bits* is the number of data bits in each character. Moreover, eight data bits are essential for one byte. The input field *String To Write* is for entering the standard command. After a delay time, the answer of the LCR-meter is shown in the *Read String* field and is updated each second. Furthermore, a file path can be quoted for the purpose of saving data output of the *Read String*. Besides, a timer is shown depending on the number of queries.

The first test of the custom made driver includes a capacitance measurement of a radial capacitor with  $C_0 = 330$  pF for 200 V stated by the manufacturer. The SCPI for reading out the capacitance is "FETC?". In figure 3.2 one example of the resulting data file is shown.



time [s];	capacity [F]
1;	+3.357430E-10
2;	+3.357413E-10
3;	+3.357354E-10
4;	+3.357305E-10
5;	+3.357253E-10

Figure 3.2: Data file of the custom made driver tested with a 330 pF capacitor.

The measurement was stopped after five queries with the result that the arithmetic average gives a capacitance value of  $C = (335.7351 \pm 0.0074)$  pF. Moreover, the accuracy for capacitance specifications of the LCR-meter (chap. 2.2) shows a deviation of  $\pm 1.6787$  pF. The measured radial capacitor is denoted with "330 pJ" meaning a capacitance of 330 pF with a tolerance of 5 % [Tra15]. Thus, the measurement is in the given tolerance range of the manufacturer.

Next, the block panel of the custom made driver will be presented to get an overview of how the VI works. The block panel (fig. 3.4) shows an outer sequence structure to save the data connected with an inner while loop to repeat the readout until pushing the stop button in the front panel.

The first part of the sequence includes the creation of a data file on a specified path. In order to fill the data file, the sending and receiving of the LCR is needed and therefore it is necessary to have a close look on it as shown in detail in the following figure:

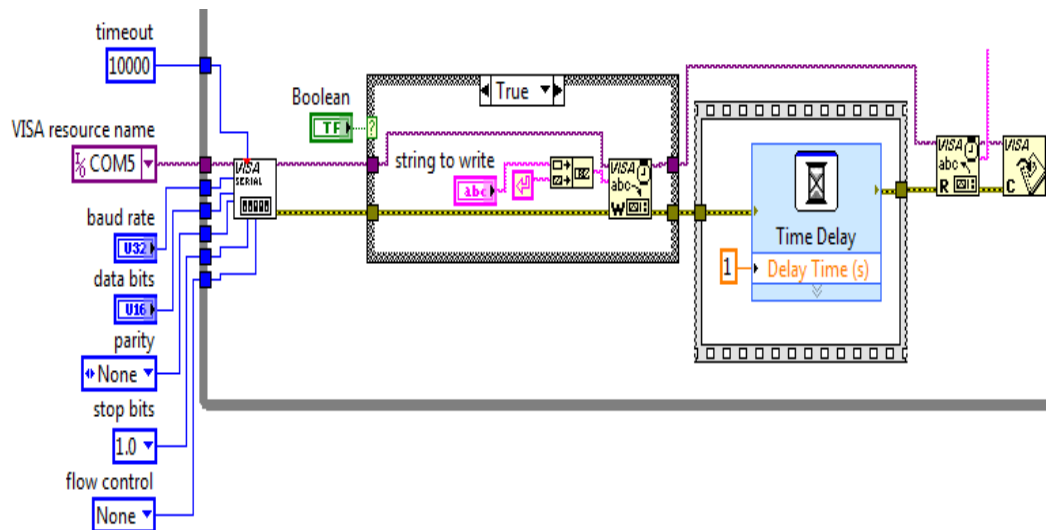


Figure 3.3: Cut of the custom made driver. After initialization of the LCR-meter, the sending end receiving of the standard command is implemented by the VISA Express-VIs.

First, the LCR-meter is initialised by the VISA serial Express-VI. The VISA serial is connected with the terminals to configure the serial port. Just *Baud Rate* and *Data Bits* are set as variable parameters, due to the fact that these are stated in the LCR manual. All other configuration terminals are set as constant, with the result that an automatic adjusted value is used. Furthermore, the USB port of the LCR-meter is required for VISA resource name of the VISA serial. After initialisation, the resource is redirected in a case structure. The case structure can be operated by the button in the front panel with the options 'true' and 'false'. The case of 'false' is empty, by contrast the case of 'true' contains the *VISA Write*. This Express-VI writes bytes to port and, therefore, needs a string to write. The other string is a constant named carriage return to complete the enter. The case structure leads to a sequence structure with a delay time of 1 s before reading. By this means, it can be prevented to read before the writing process is finished. The *VISA Out* Express-VI is used to close the session to port.

The measured and every second updated capacitance value is saved with the ongoing number of loops in the data file as seen in the following block panel. Next, the custom made driver can be tested at a levelmeter in a liquid nitrogen reservoir presented in the next section.

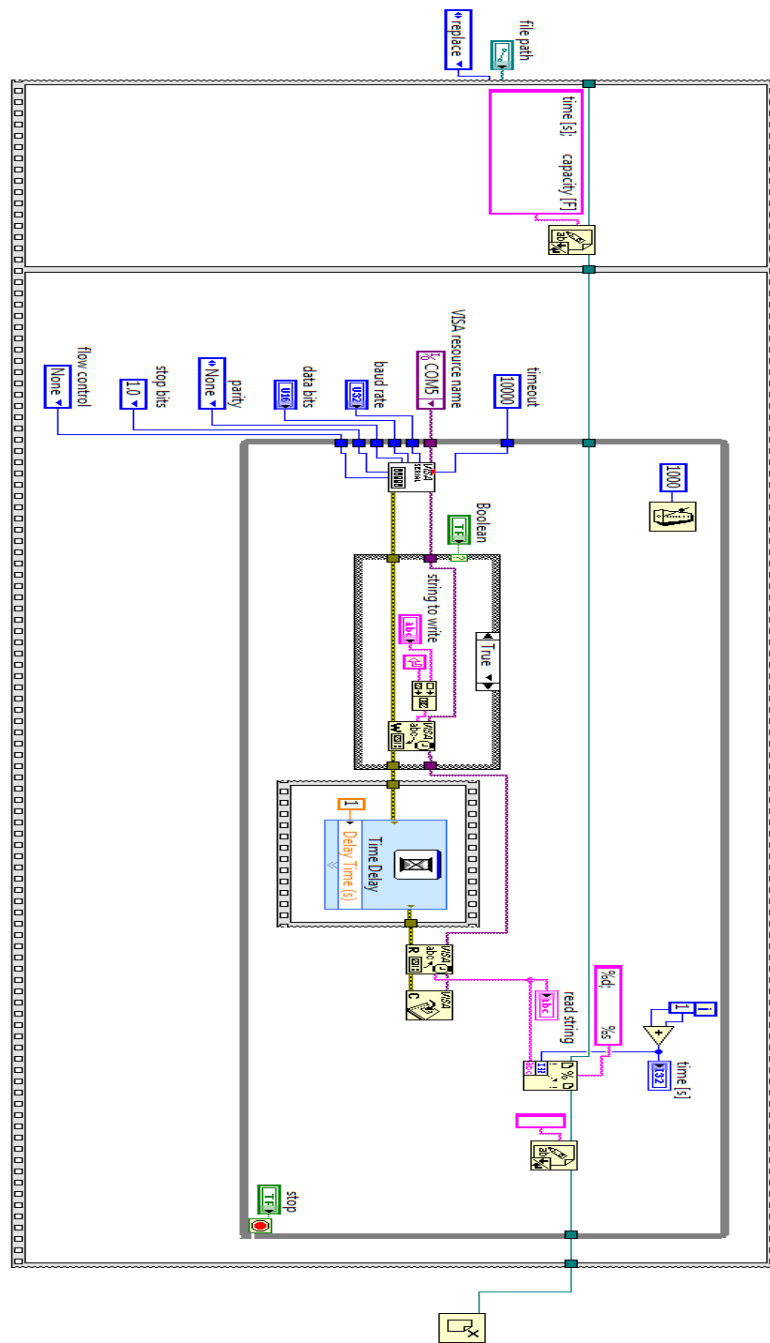


Figure 3.4: Total block panel of the custom made driver. The outer sequence structure is for creating a data file connected with an inner while loop for querying the LCR-meter until the stop button will be pushed.

### 3.3 Capacitance Measurement of a Levelmeter with the Custom Made Driver in Liquid Nitrogen

In order to test the custom made driver VI, a levelmeter was used similar to the ones of the TPC but with other dimensions:  $l = 55$  mm,  $D = 10$  mm,  $d = 9$  mm. The levelmeter was mounted in a cylindrical vessel filled with liquid nitrogen and a folding rule was affixed to take readings of the filling height. Furthermore, a weighting device was used to document the weight decrease during vaporization due to the considerably smaller weighting device standard error of  $\pm 0.1$  g in contrast to the large reading error ( $\pm 1$  mm) of the folding rule.

In the beginning, the levelmeter was fully covered by liquid nitrogen. During the vaporization, the liquid level is reduced and as consequence, the capacitance changed according to equation 2.7. Similarly, the mass of the filled vessel is reduced as seen in figure 3.5.

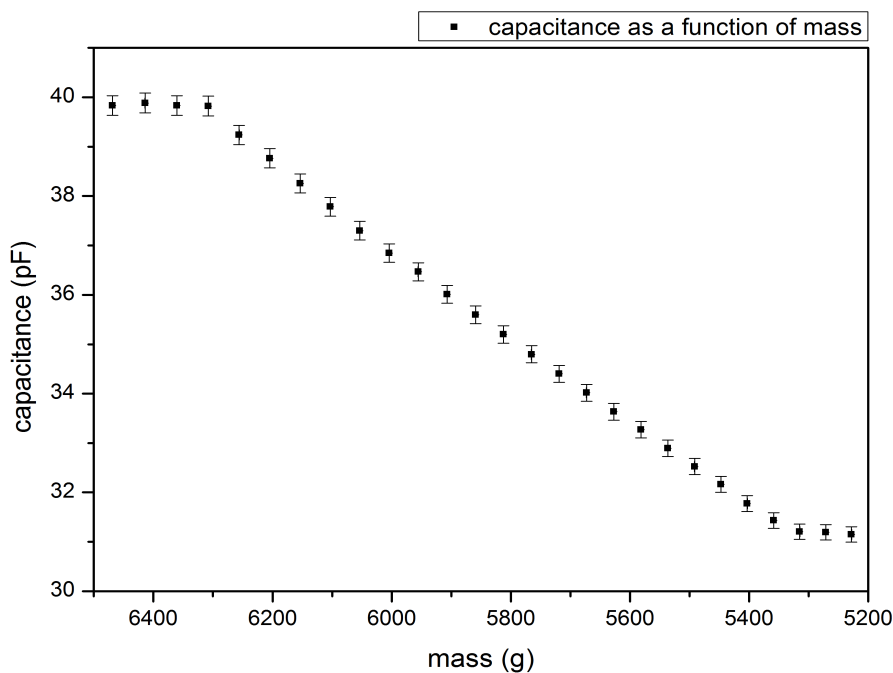


Figure 3.5: Change in capacitance as a function of mass during vaporization.

Obviously, the change point between the full and slowly emptying levelmeter as well as between the slowly emptying and the quite empty levelmeter is shown. As soon as the levelmeter is not covered by any liquid, the capacitance is not changing anymore. Furthermore, figure 3.5 shows an empty levelmeter capacitance of about  $C_0 = (31.14 \pm 0.16)$  pF. This offset is a consequence of the cables between levelmeter and LCR-meter. Nevertheless, not the offset is of further interest, but the relative change of capacitance. The clearly visible error bars of the capacitance result out of the aforementioned accuracy of the LCR. However, the mass error bars are too small to see in the figure.

In order to make use of this precision, the mass is plotted against the filling height shown in figure 3.6.

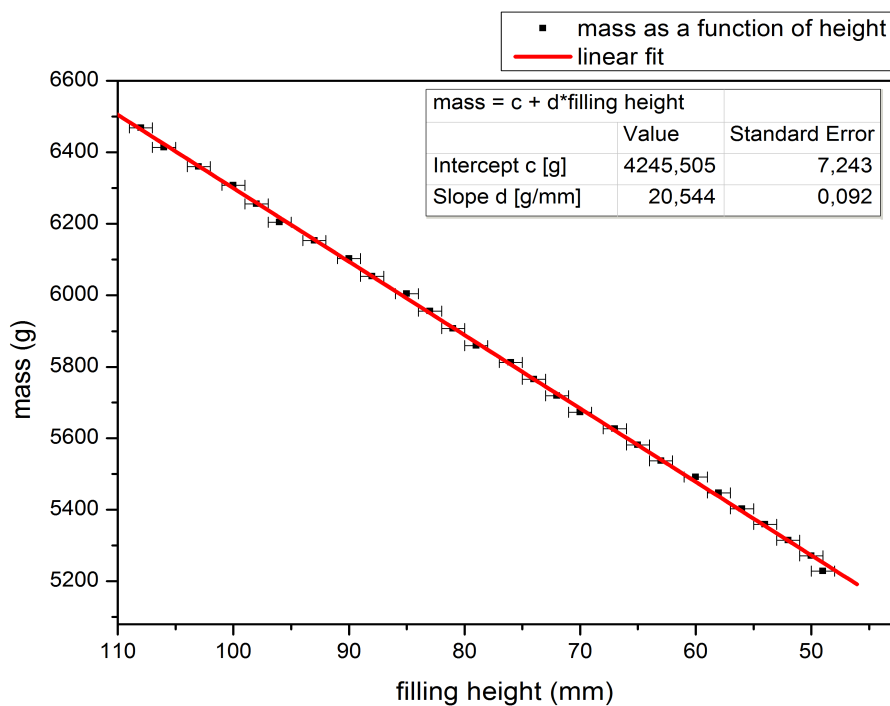


Figure 3.6: Vessel mass as a function of the  $\text{LN}_2$  filling height during vaporization.

According to the expectations, a linear connectedness between mass and filling height decrease can be found. By this means, the linear fit equation out of figure 3.6 offers the

converting direction,

$$\text{mass} = c + d \cdot \text{filling height}, \quad (3.1)$$

between mass and filling height, with a  $c$  and  $d$  defined as shown in the figure. As a consequence, the capacitance change as a function of mass (fig. 3.5) can be converted into a capacitance change as a function of filling height illustrated by figure 3.7).

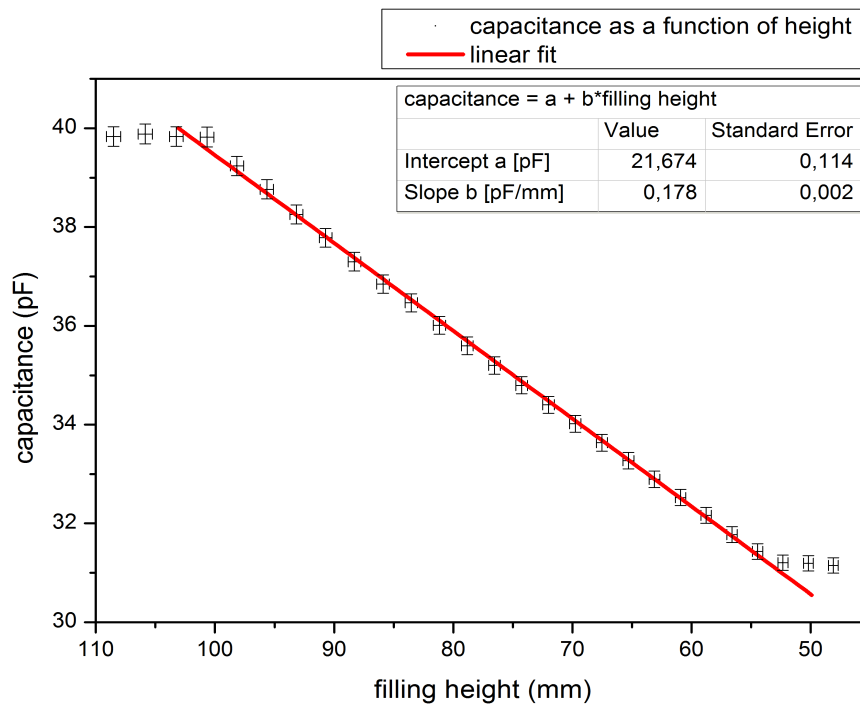


Figure 3.7: Change in capacitance as a function of the filling height during vaporization.

Due to the error propagation out of the converting direction (eq. 3.1)

$$\Delta \text{filling height} = \sqrt{\left(\frac{1}{d} \Delta \text{mass}\right)^2 + \left(\frac{1}{d} \Delta c\right)^2 + \left(-\frac{\text{mass} - c}{d^2} \Delta d\right)^2},$$

the filling height standard error is considerably smaller than the reading error of the folding rule. The error could be reduced by about 50 %. Therefore, the result of the change in capacitance per filling height out of the linear fit in figure 3.7 has improved. The slope  $b$  can be compared with the theoretical capacitance per length change of this levelmeter (eq. 2.10):

Table 3.1: Comparison of the theoretical capacitance change and the experimental change out of the fit slope  $b$  (fig. 3.7).

theoretical change in capacitance $\frac{\Delta C_t}{mm}$	$(0.247 \pm 0.035)$ pF/mm
experimental change in capacitance $\frac{\Delta C_e}{mm}$	$(0.178 \pm 0.002)$ pF/mm

The deviation of over 25 % can be explained by the non-consideration both of the 1 mm slit in the tube and the temperature and pressure dependence of the dielectric constants [MaB01]. Another significant point is that the oxygen concentration of the surrounded air should be considered, too. Accordingly, a qualitative statement can not be made, but is not necessary either. Considering that the custom made driver was successfully tested, the implementation to readout the three levelmeters of the TPC is needed and will be presented in the following section.

### 3.4 Levelmeter Read-Out Set-Up for the Münster TPC

The upgrade of the custom made driver for the TPC levelmeter read-out and the hardware set-up to switch between the levelmeters as well as already shown in figure 2.4 is illustrated in the following.

In order to readout the three levelmeters of the TPC with the aforementioned custom made driver, an arduino board in combination with a relais circuit provides a low cost facility. The board is based on the ATmega328P and has both a lot of digital and analog pins [Ard16]. The arduino is connected with a home-made three-switches relais circuitry (fig. 3.8). Just one pin at a time can be gated and the capacitance of the specified levelmeter is readout by the LCR-meter. If no pin is gated, in other words if all switches are open, an empty capacitance of about  $C_0 = (11.48 \pm 0.06)$  pF is measured.

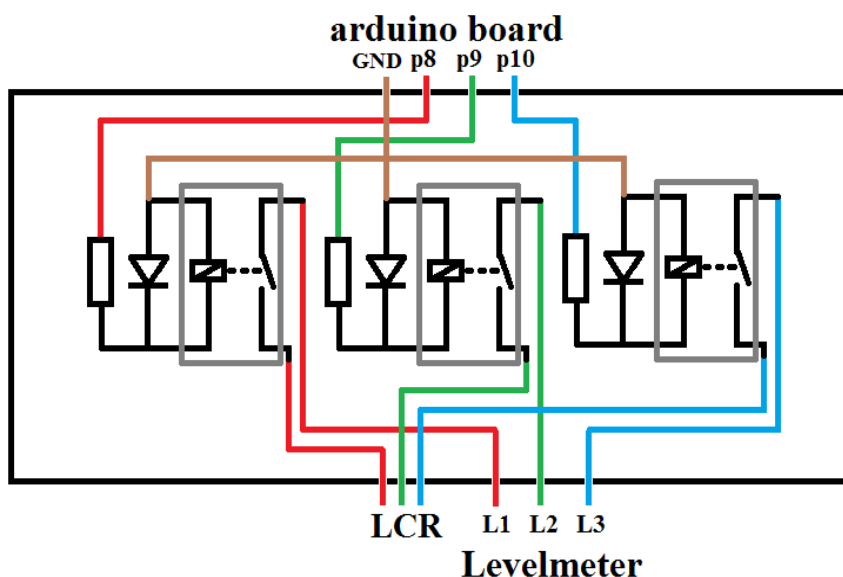


Figure 3.8: Three-switches relais circuitry. If a pin is gated, the relais connects the specified levelmeter with the LCR-meter with the result that the capacitance of the levelmeter can be readout.

The circuit is composed of an resistor, a protective diode and a relais for each pin. The diodes prevent arcing because if a relais is gated by a transistor and the exciting voltage is off, the collapsed magnetic field produces a voltage oriented against the exciting

voltage. This leads to the case, that the switching transistor sees a collector voltage with a false polarity. As a consequence, the transistor will be damaged. In order to prevent this process, a reverse-biased catch diode is added and the inductive reverse voltage is short-circuit.

In order to use the relais circuit and the arduino board for a levelmeter switch, the three pins of the arduino have to be controlled by the custom made driver. For this purpose, the fact that LabVIEW possesses an arduino library is most helpful and therefore an arduino sub-VI was built with the arduino Express-VIs of the library (fig. 3.9).

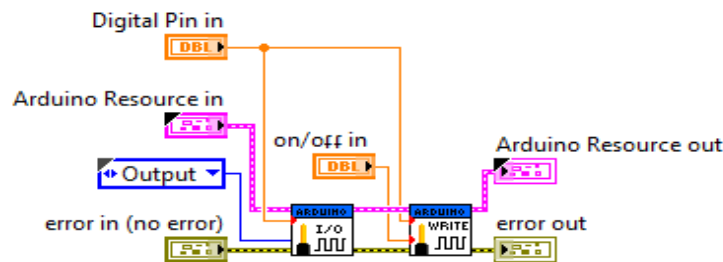


Figure 3.9: Self-made *arduino* Sub-VI to gate different pins of the micro-controller.

The sub-VI is composed of two arduino Express-VIs. The *Set Digital Pin Mode* is used to configure the pin, which contains the specified number of the pin and the configuration of input or output. The *Digital Write Pin* is utilized to set the digital output pin to on or off. For the simple reason that pin-switching is needed, the pin number input and the on/off input are set as variable input parameters. By this means, a specified pin can be gated, the combined levelmeter is readout and the next pin can be gated afterwards until each levelmeter capacitance is measured. According to that, the whole blockpanel of the final TPC levelmeter read-out driver (fig. 3.12 and more distinct in the appendix) is composed to all intents and purposes of alternating pin-switching sequences (fig. 3.9) and sending and receiving sequences (fig. 3.3), with the result that the three levelmeters are readout consecutively. In addition, the final TPC levelmeter read-out driver was optimized further on. For reasons of clarity and comprehensibility, some parts of the blockpanel were dropped into sub-VIs as seen in the appendix. Furthermore, the measured capacitance values are averaged about each five seconds before saving. Besides, the VI was extended with the result that a new data file is created each day and moreover a live plot for each levelmeter is added in order to simplify the monitoring.

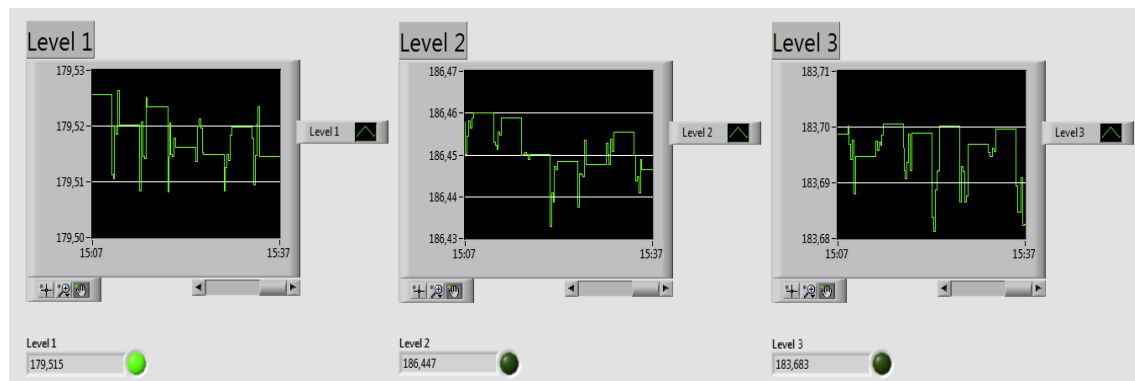


Figure 3.10: The frontpanel of the final levelmeter read-out for the Münster TPC. Three live-plots acquire the capacitance change of the levelmeters. The stepped form results out of the series connection of the levelmeters.

The frontpanel of the VI (fig. 3.10) shows the three live-plots of the levelmeters. Due to the series connection of the three levelmeters, the live-plots have a stepped form, since during the measurement of the second and third levelmeter, the live-plot of the first levelmeter plotted the last measured capacitance value further on. The plots process the averaged capacitance values by a local variable (fig. 3.11). The while loop was made by Michael Murra for the Slow Control of the Münster TPC gas system and was allowed to take on. In addition, the readout levelmeter is displayed by a LED beside the measured capacitance value for reasons of clarity and all configurations of the LCR and settings like the file path are set as constant as seen in the frontpanel.

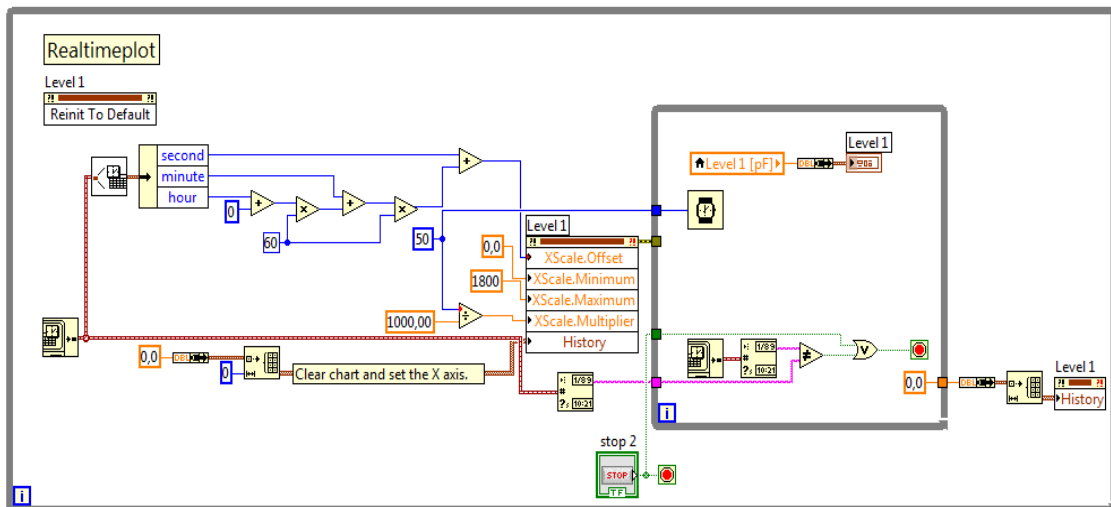


Figure 3.11: Block panel cut of the TPC levelmeter readout driver. The while loop processes the averaged capacitance values into a real-time live plot. Made by Michael Murra.

Consequently, both the hardware set-up and the LabVIEW-based driver to switch between the three levelmeters were realized, with the result that different capacitance measurements of the TPC could be made presented in the following chapter.

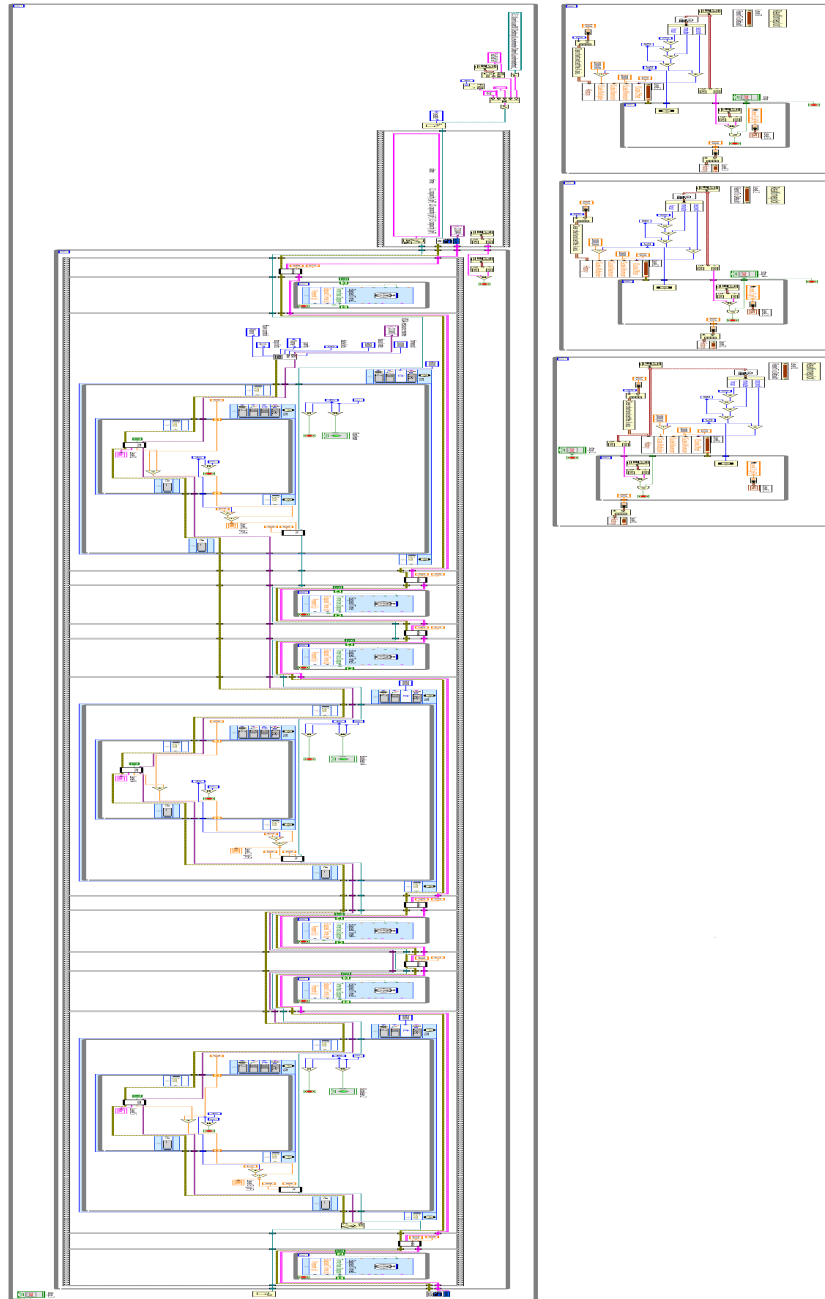


Figure 3.12: Blockpanel of the final levelmeter read-out for the Münster TPC. The iterative sequences, which differentiate just in the digital pin number and the constant-set input of the data saving, and the live plots are omitted. Some sub-VIs are created for a better clearness. After readout each levelmeter, the sequence structure repeated oneself until the loop is stopped at the next day by the date comparison. Accordingly, the data file and the arduino can be closed and the whole VI is repeated.

## 4 Capacitance Measurements of the Münster TPC Levelmeters

This chapter shows several capacitance measurements of the three Münster TPC levelmeters. At first a calibration of the levelmeters by measurements of TPC filling and recuperation will be presented. Moreover, the stability of the liquid xenon level of the Münster TPC, which is important for the operation of dual phase TPCs, will be shown.

### 4.1 Calibration of the Levelmeters during Filling and Recuperation

After connecting the hardware set-up with the TPC as shown in figure 2.4, the calibration of the levelmeters by filling the TPC with liquid xenon has been performed. The TPC was continuously filled at a constant flow rate of 5 standard liter per minute (slpm) and the capacitances of the three levelmeters were readout during ongoing xenon liquefying by the VI with the relais circuitry. As soon as a ramp of the capacitance is manifested, enough xenon is liquefied so that the liquid reached up to the lower end of the levelmeters and filled them. Figure 4.1 shows the measured change in capacitance of the three levelmeters as a function of time.

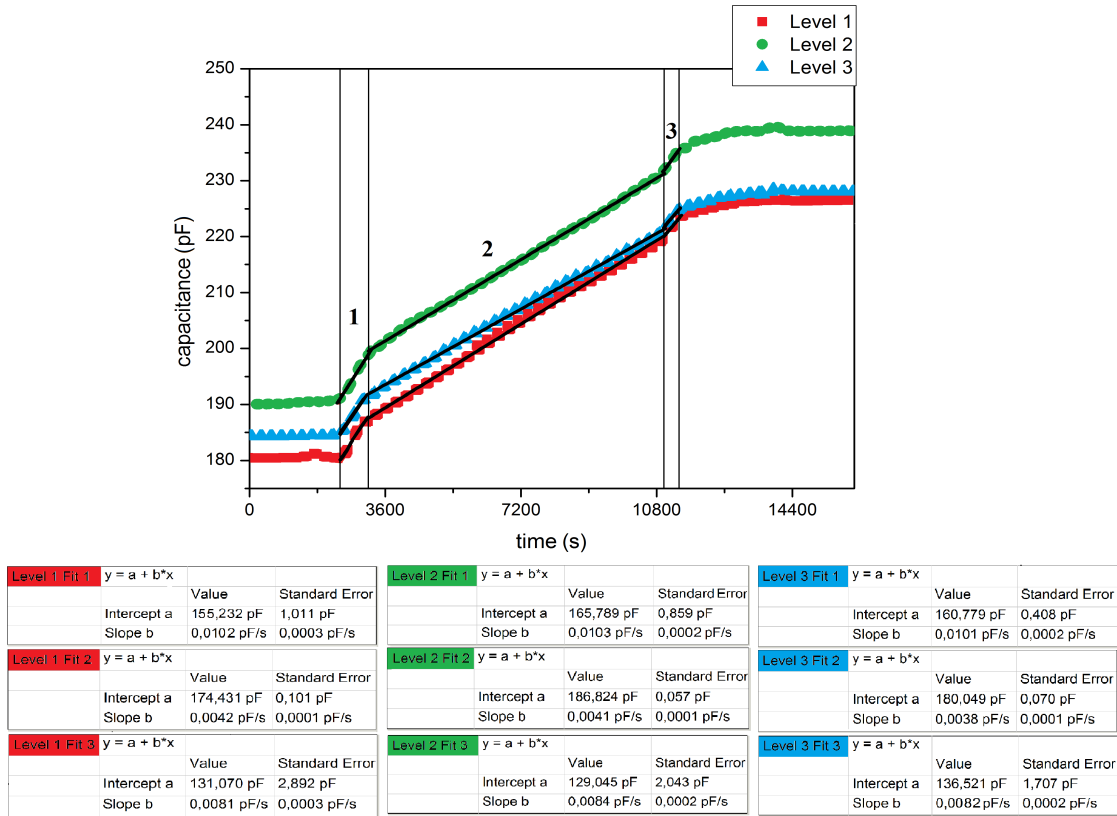


Figure 4.1: Capacitance measurement of the TPC filling to calibrate the levelmeters.

Conspicuously, the three levelmeters have a different offset. This occurs due to different cable lengths of the levelmeter implementation. Due to the fact that just relative changes are attractive for the calibration no further attention is given to the offset. Moreover, figure 4.1 shows, three different areas of the slope can be identified. In addition, the capacitance change of levelmeter 3 is remarkable. In area 1 and 3, the slope seems to be equal to those of the other meters, but the slope of area 2 seems to be distinctly lower.

The three different areas are fitted independently of one another. First, the capacitances of the levelmeters increase rather steep, therefore a faster increase of the liquid level is assumed. Afterwards, all three levelmeters display a flatter rise of capacitance for more than two hours of filling. The assumption of levelmeter 3's distinctly lower slope in area 2 can be confirmed by the slope of  $b_3 = (0.0038 \pm 0.0001) \text{ pF/s}$  in contrast to  $b_1 = (0.0041 \pm 0.0001) \text{ pF/s}$  for levelmeter 1 and  $b_2 = (0.0042 \pm 0.0001) \text{ pF/s}$  for

levelmeter 2.

Afterwards, the change in capacitance of the levelmeters is increased again in area 3. Subsequently, the change converges slowly to a maximum capacitance, which can be explained by a careful turn down of the flow to prevent an overflow and therefore a damage of connections gone into the TPC. A maximum capacitance means a fully filled levelmeter. The verification of a full-filled meter can be done by the example of levelmeter 2 and the comparison with the expected total capacitance for a fully filled cylinder (eq. 2.9): the data file of the measurement shows, levelmeter 2 converges at a maximum capacitance of  $C_{2,max} = (238.85 \pm 1.19)$  pF. Using the beginning capacitance  $C_{2,min} = (188.95 \pm 0.94)$  pF, a total change in capacitance of  $C_{2,t} = (49.9 \pm 1.52)$  pF is found. The deviation is given by the error propagation

$$\Delta C_{2,t} = \sqrt{(\Delta C_{2,min})^2 + (-\Delta C_{2,max})^2}.$$

Compared with the expected total capacitance for a levelmeter filled to capacity  $C_{max} = (49.918 \pm 0.072)$  pF, the assumption that the levelmeters were fully filled can be confirmed.

Moreover, a look to the inner design of the TPC (fig. 4.2) may clarify the three fitted areas.

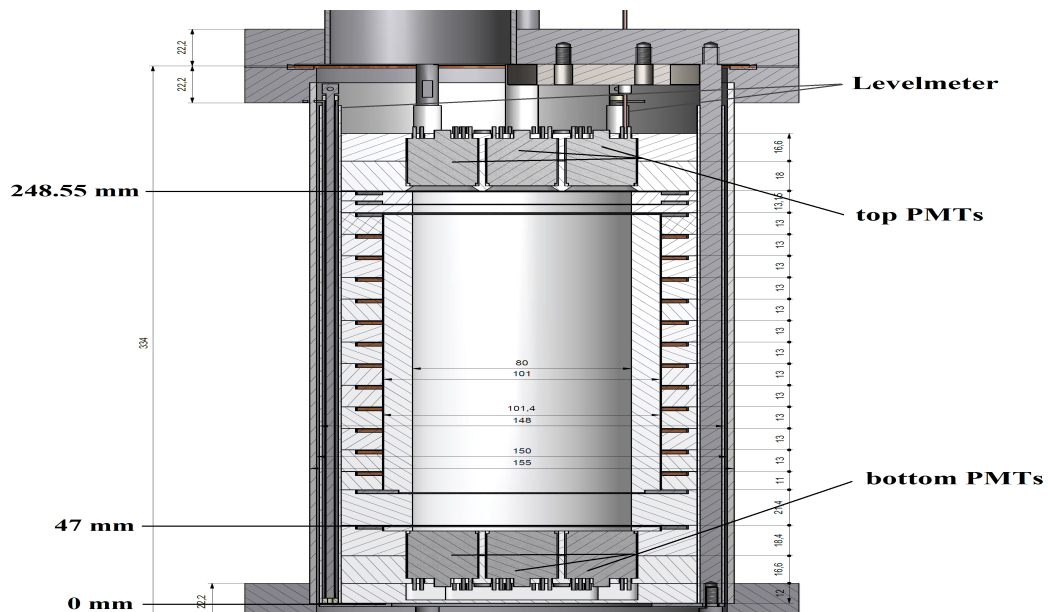


Figure 4.2: TPC Overview by C. Huhmann

The first steep slope of each levelmeters change in capacitance can be explained due to the PMT array on the bottom of the TPC. In this area the volume to a designated filling height is filled faster because the PMTs suppress volume. At a filling height of 47 mm the PMTs are completely surrounded by liquid xenon and a bigger volume is needed to be filled by liquid. Therefore, a flatter slope of capacitance rise is expected. This can be verified compared with figure 4.1. The xenon volume had to be filled constantly until a filling height of 248.55 mm has been reached. At this height the array of the top PMTs leads to a smaller filling volume again. Thus, the second point of changing the slope can be explained.

The intersection points of the linear equations in figure 4.1 are correlated with the design of the inner TPC. Due to the constant filling the increase of filling height is linear with time and thus also the capacitance change. Accordingly, the accurate identification of these three areas and the specification of the inner design can be used to convert the time interval into a filling height interval (fig. 4.3).

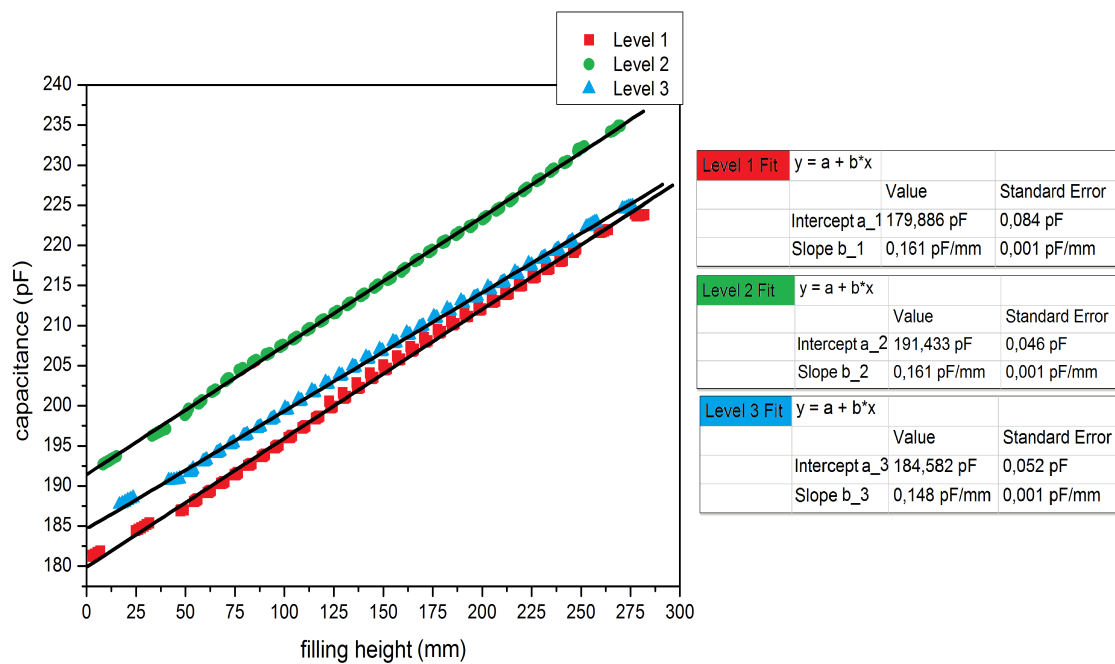


Figure 4.3: Capacitance as a function of the filling height. The identification of different filling areas leads to a converting from a time interval to a filling height interval.

As seen in the figure 4.3, the correlation with the inner design leads to a linear increase of the capacitance per filling height of the TPC illustrated by linear fits with a slope of  $b_1 = b_2 = (0.161 \pm 0.001)$  pF/mm for levelmeter 1 and levelmeter 2 and  $b_3 = (0.148 \pm 0.001)$  pF/mm for levelmeter 3. Therefore, levelmeter 3 is different to the expectations. The graph shows, at a filling height of about 100 mm the constant slope seems to decrease in comparison to the other two levelmeters as hinted in figure 4.1. The slope of the linear fit equation of each levelmeter can be compared with the expected slope of  $(0.170 \pm 0.024)$  pF/mm value as calculated in equation 2.8. According to this, the comparison gives a deviation of 5.6 % for levelmeter 1 and 2 and about 13 % for levelmeter 3. Noticeably, the levelmeters of the TPC deviate from the theoretic predicted value of the change in capacitance per millimeter not as much as the levelmeter of the nitrogen measurement outside the TPC in chapter 3.3. An advantage unlike the LN<sub>2</sub> measurement is that the levelmeters in the TPC are surrounded completely with xenon because of the isolated system. A deviation of about 5 % seems to be acceptable, since side effects as the 1 mm slit of the levelmeter design along the tube was neglected for calculations. The 13 % of levelmeter 3 can not be explained at this moment. Possibly, an inaccurate manufacturing leads to those deviations, but in order to make a clear statement further measurements are needed.

Next, a recuperation starting at a dual phase mode will be presented to compare the slopes of TPC filling and recuperation.

In dealing with the TPC, but principally with the recuperation, it is absolutely necessary to take great care of the explosive expansion of gas during the vaporization, therefore, the recuperation of the TPC is done with a constant circulation of the gas system. Thus, xenon is extracted with a flow of about 3 slpm. The exact flow is taken out of the flow control data.

In order to compare the capacitance change of the recuperation and the filling, the time axes can be adjusted to a constant flow of 5 slpm. Taking into account that the filling of the TPC has been performed with a constant flow of 5 slpm and the recuperation has been done at a constant flow of 3 slpm, the time axis of the recuperation data has been normalized to the filling data by a stretching factor of 3/5.

Therefore, the normalization of the time axis is achieved by a multiplier of the specified flow out of the slow control data divided by 5 slpm. Since three different areas of filling reposed on the inner design of the TPC have been identified further up, the same is expected to emerge at the recuperation. Incidentally, the following graph shows the recuperation starting at a dual phase level, thus just two different areas are expected.

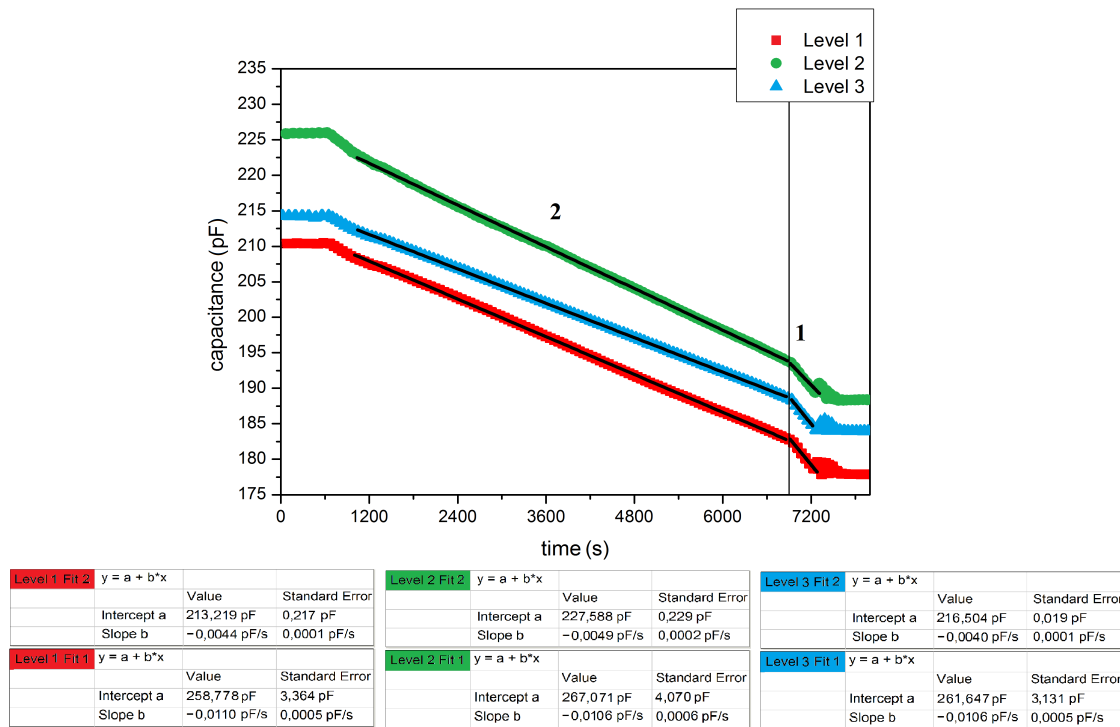


Figure 4.4: Recuperation of the TPC with normalized flows. The normalization is done by a multiplication of the time axes with a multiplier of the specified flow divided by 5 standard liter per minute.

Figure 4.4 shows that the constant capacitance of each levelmeter decreases at the same time. The recuperation starts and the levelmeters are emptied constantly. After a while, a distinct change can be seen. The decrease of the change in capacitance intensifies until the capacitances converge. The resulting two different parts were fitted independently of each other. In doing so, a few minutes after starting and before the convergence of the capacitance are not considered due to the fact that the removing of the equilibrium between liquefying and vaporization needs some time.

The first slope shows the middle part of the TPC, therefore can be confronted with the middle one of the filling graph. The second slope represents the TPC area with the PMT array on bottom similar to the first slope of the filling. Since the recuperation is started at a dual phase mode, no slope of the TPC top area exists to compare with the correspond slope of the filling. The comparison of the different slopes is resumed and displayed in table 4.1.

Table 4.1: Comparison of the filling slope and the recuperation slope

Levelmeter	TPC area	Filling Slope [ $10^{-3}$ pF/s]	Recup Slope [ $-10^{-3}$ pF/s]
level 1	bottom (1)	10.2( $\pm$ 0.3)	11.0( $\pm$ 0.5)
	middle (2)	4.2( $\pm$ 0.1)	4.4( $\pm$ 0.1)
	top (3)	8.1( $\pm$ 0.3)	-
level 2	bottom (1)	10.8( $\pm$ 0.2)	10.6( $\pm$ 0.6)
	middle (2)	4.1( $\pm$ 0.1)	4.9( $\pm$ 0.2)
	top(3)	8.4( $\pm$ 0.2)	-
level 3	bottom (1)	10.1( $\pm$ 0.2)	10.6( $\pm$ 0.5)
	middle (2)	3.8( $\pm$ 0.1)	4.0( $\pm$ 0.1)
	top (3)	8.2( $\pm$ 0.2)	-

Table 4.1 shows, the slopes of filling and recuperation are in the same order of magnitude and therefore, the behaviour of the levelmeters at the filling is similar to the behaviour at the recuperation. Deviations can be explained by the different modes of filling and recuperation. The recuperation is done by permanent circulation of the gas system contrary to the filling. Conspicuously, levelmeter 2 and levelmeter 3 possess the same slope at the bottom of the TPC during recuperation, whereas the slopes of the middle area during recuperation is widely different. Even more remarkable: the slope of the TPC top area of each levelmeter is flatter than the slopes of the bottom. Such deviations can not be explained at this moment.

In conclusion, the calibration of the Münster TPC levelmeters during filling and recuperation was successful. At the first TPC filling measurement, three different filling areas of the inner TPC volume could be identified and in comparison with the exactly TPC dimensions of the inner xenon vessel, a change in capacitance per filling height of the levelmeters could be found. The recuperation could verify two of the areas. However, the third slope could be not identified because the recuperation was started at a dual phase mode. In this mode, not only the knowledge of the filling height is of importance, but also the stability of the liquid level over time. Thus, a stability analysis during a dual phase operation has been done and is presented in the next section.

## 4.2 Stability of Liquid Level during Operation

As mentioned in chapter 2.1, the knowledge of the precise liquid xenon level is important for the operation with the TPC due to the small distance of the grounded gate mesh and the anode mesh of a few millimeters. According to this, the stability of the liquid level has to be guaranteed and is therefore analyzed in the following.

After filling, the liquid xenon level is reduced to a stable filling height at the gate mesh level with  $h = 235.40$  mm while the capacitance related to the liquid level at the gate mesh can be calculated for each levelmeter with the relative capacitance change out of the calibration. Due to the fact that the circulation was increased after liquid level reducing to the level of the gate mesh, the equilibrium needs some time to set. Figure 4.5 shows the reduction of the liquid level to the dual phase and the analyzed part for stability of the liquid level in dual phase mode.

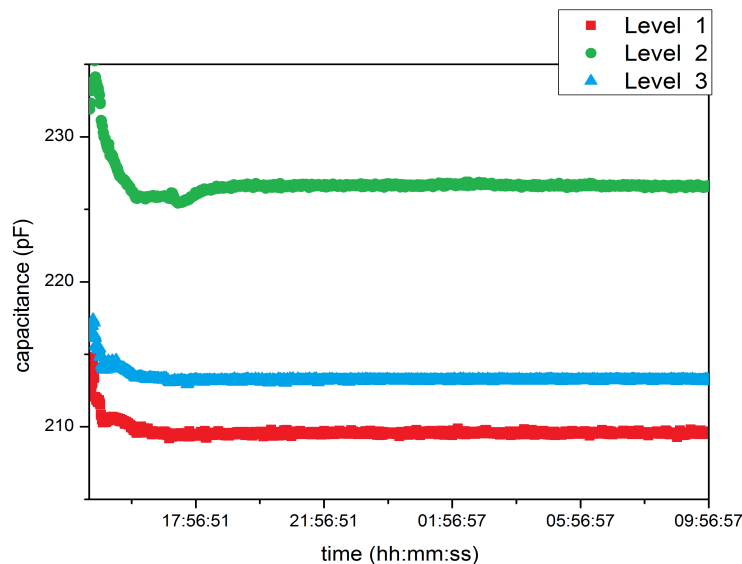


Figure 4.5: Levelmeter capacitances as a function of time of the Münster TPC. After reducing the liquid level up to a dual phase mode of the TPC, the stability can be analyzed.

In order to analyze the stability, each levelmeter is examined individually. The different capacitance values were displayed in a histogram with the counts of the capacitance values binned in an area of 0.02 pF. The distribution of the binned capacitance values is fitted by a Gaussian function, with the result that the counts are plotted as a function of the standard deviation.

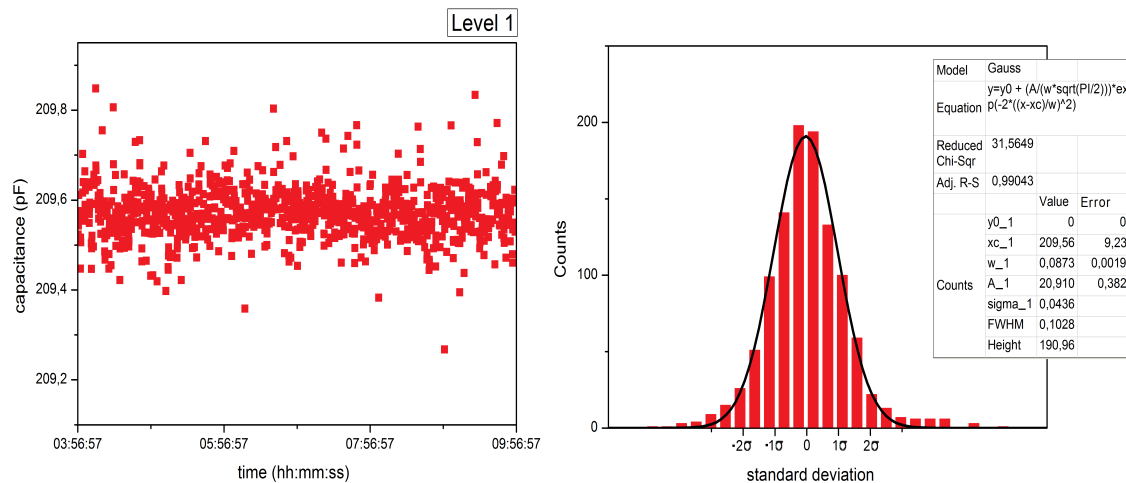


Figure 4.6: Capacitance measurement of levelmeter 1. On the left: the level 1 capacitance measurement of six hours in dual phase mode out of figure 4.5 is shown. On the right side: the distribution of the binned capacitance values. A Gaussian fit verified the normal distribution and shows the standard deviation.

Figure 4.6 shows the stability of the liquid xenon level in the TPC at the level of the gate mesh by reference to capacitance measurements of levelmeter 1. The Gaussian fit of the binned capacitance values results in a sigma of  $\sigma_1 = 0.0436$  pF. The  $w$  of the Gaussian fit equation  $y = y_0 + A/(w \cdot \sqrt{\pi/2}) \cdot e^{-2 \cdot ((x-x_c)/w)^2}$  corresponds to two sigma and the two standard deviations from the mean accounts a confidence level of 95.44 % [Cim13].

As a consequence, a levelmeter precision  $P_1$  with a confidence level of two sigma can be calculated about

$$P_1 = \frac{w_1}{b_1} = (0.54 \pm 0.01) \text{ mm},$$

with the slope  $b_1 = (0.161 \pm 0.001)$  pF/mm of levelmeter 1 out of the calibration in figure 4.3,  $w_1 = (0.873 \pm 0.0019)$  pF and the error propagation

$$\Delta P = \sqrt{\left(\frac{1}{b} \cdot \Delta w\right)^2 + \left(-\frac{w}{b^2} \cdot \Delta b\right)^2}. \quad (4.1)$$

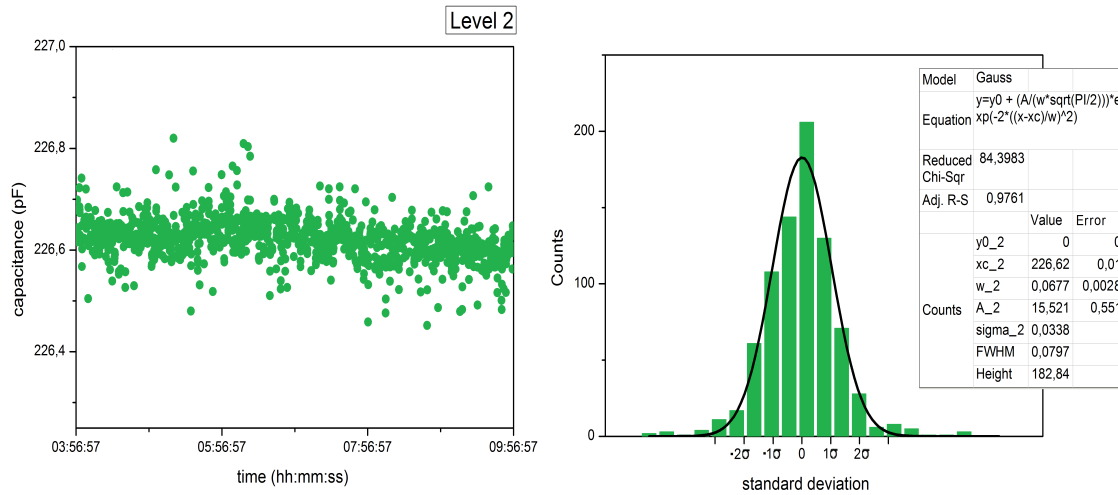


Figure 4.7: Capacitance measurement of Levelmeter 2. On the left side: the zoom in of six hours capacitance measurement with levelmeter 2 is displayed. On the right side: the distribution of the measured capacitance values was fitted by a Gaussian. As a consequence, the counts of the capacitance values can be shown as a function of the standard deviation.

As figure 4.7 shows, levelmeter 2 seems to have a higher precision, because the standard deviation  $\sigma_2 = 0.033$  pF is smaller with the same change in capacitance per millimeters  $b_2 = (0.161 \pm 0.001)$  pF/mm out of the calibration graph (4.3). Accordingly, a precision of

$$P_2 = \frac{w_2}{b_2} = (0.41 \pm 0.02) \text{ mm}$$

is given. Calculated with the  $w_2 = (0.0667 \pm 0.0028)$  pF of the Gaussian fit in figure 4.7 and the same error propagation as aforementioned.

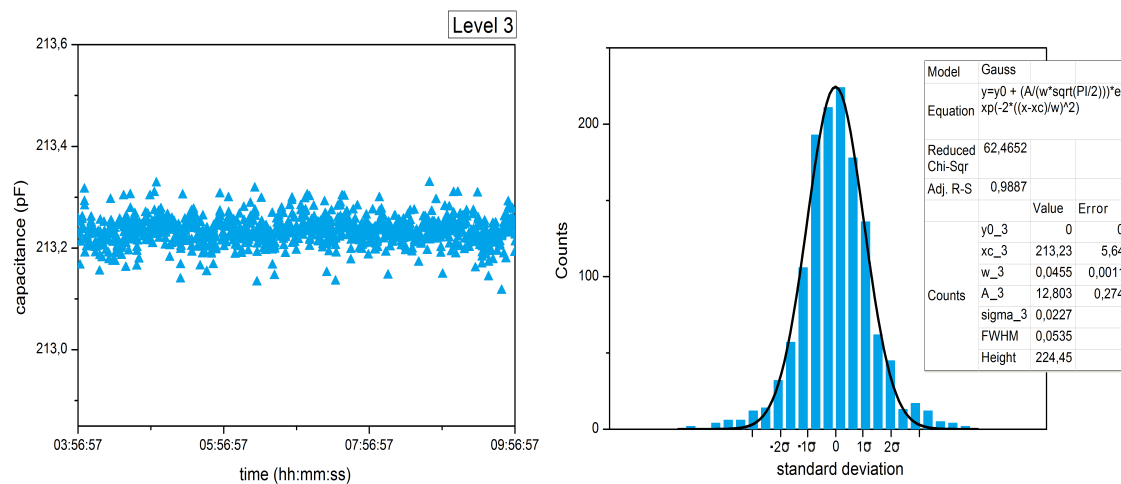


Figure 4.8: Capacitance measurement of Levelmeter 3. On the left: the level 3 capacitance measurement of six hours in dual phase mode of figure 4.5 is displayed. On the right side: the distribution of the measured capacitance values is depicted. A Gaussian fit verified the normal distribution and shows the standard deviation.

The Gaussian fit out of figure 4.8 gives a standard deviation of  $\sigma_3 = 0.0227$  pF and a  $w_3 = (0.0455 \pm 0.0011)$  pF. In combination with the slope  $b_3 = (0.148 \pm 0.001)$  pF/mm, the resulting precision for levelmeter 3 is

$$P_3 = \frac{w_3}{b_3} = (0.31 \pm 0.01) \text{ mm},$$

calculated again with the error propagation in equation 4.1.

In conclusion, the three levelmeters possess a precision in the scale of sub-mm. Therefore, the liquid level can be adjusted exceedingly exact on a specified level and in addition can be kept on this level with a precision in scale of sub-millimeters.

## 5 Conclusion and Outlook

In the following, the results of this bachelor thesis will be summed up and an outlook will point further research out.

A precise liquid xenon level is essential for the operation with a dual phase time projection chamber due to the small difference between the grounded gate mesh and the anode mesh. Since exactly at this area in between, the electrons are accelerated into the gaseous phase. In order to get an optimum yield of extracted electrons, the best liquid xenon level need to be found. For this purpose, the Münster Xenon Group have implemented three cylindrical capacitors which change their capacitance with the filling height of liquid xenon.

Within the framework of this bachelor thesis, a Münster TPC levelmeter read-out has been created. The capacitances of the levelmeters have been readout with a conventional handheld LCR-meter and in order to submit the data to the computer, a LabVIEW-based driver for the LCR-meter have been created.

Since there are three implemented levelmeters, an opportunity to switch between the three levelmeters has been found and realized by an arduino board in combination with a relais circuitry. The controlling of the arduino board has been implemented into the LabVIEW VI of the read-out showing the result that the levelmeters have been readout consecutively. The monitoring has been achieved by three live plots which have plotted and displayed the measured capacitances in real-time.

A calibration of the first levelmeter measurement of TPC filling has been done by reference to the inner design of the TPC and as consequence, levelmeter 1 and 2 have had a change in capacitance per millimeter of  $b_1 = b_2 = (0.161 \pm 0.001)$  pF/mm and levelmeter 3 a change of  $b_3 = (0.148 \pm 0.001)$  pF/mm.

Afterwards, the recuperation of the liquid xenon had to be able to verify the correlation with the inner TPC design, so that any wrong assumption has been excluded.

Finally, the stability of each levelmeter has been analyzed with the help of calibration. For this purpose, the liquid xenon level has been reduced after filling to the level of the grounded gate mesh, since this level is the operation level of the TPC. The level stability during a time interval of six hours has been analyzed and subsequently, a precision of the three levelmeters in range of sub-millimeters has been found. Accordingly,

Levelmeter 1 has possessed a precision of  $P_1 = (0.54 \pm 0.01)$  mm, Levelmeter 2 has had a precision of  $P_2 = (0.41 \pm 0.02)$  mm and levelmeter 3 has achieved a precision of  $P_3 = (0.31 \pm 0.01)$  mm at a confidence level of 95.44 %.

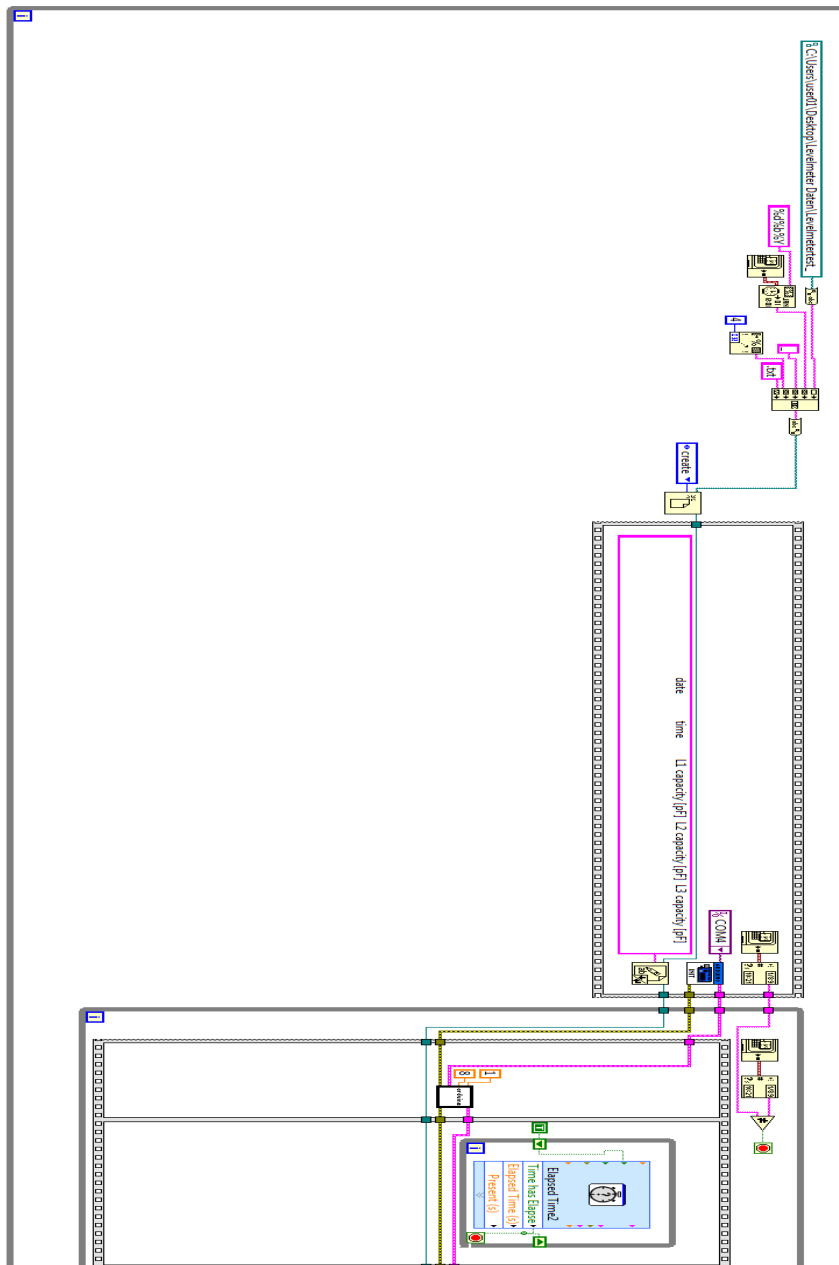
In future, this resolution will be used to make S2 measurements with a radioactive source at different levels, with the result that the level with the highest electron yield will be found.

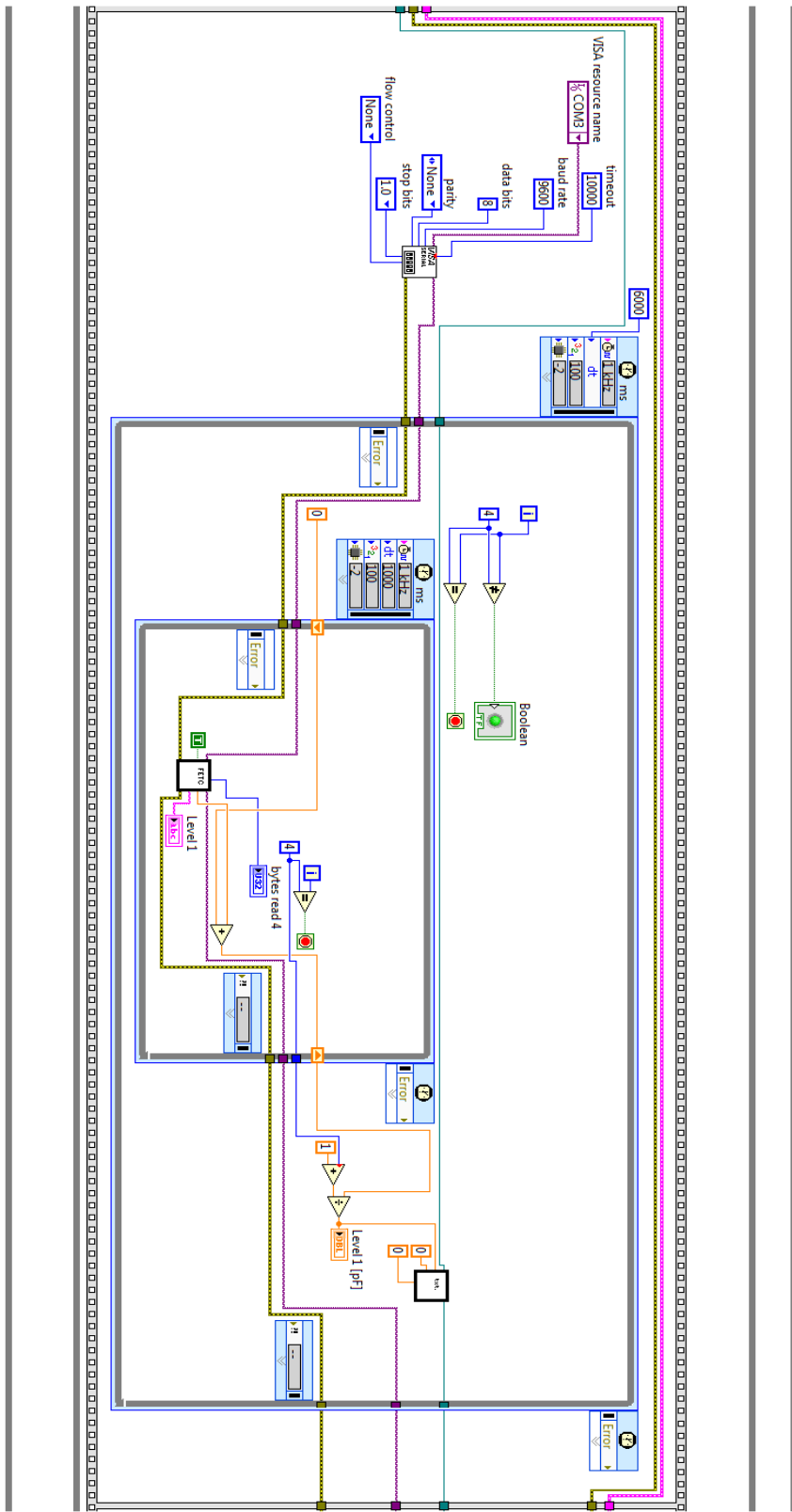
In addition, the hardware set-up including the LCR-meter with its battery, the arduino board and the relais circuitry will be mounted in a box for reasons of elegancy and clarity. Besides, points of contact with cables and other hardware will be prevented by this means, which is of advantage for capacitance measurements in scale of picofarad.

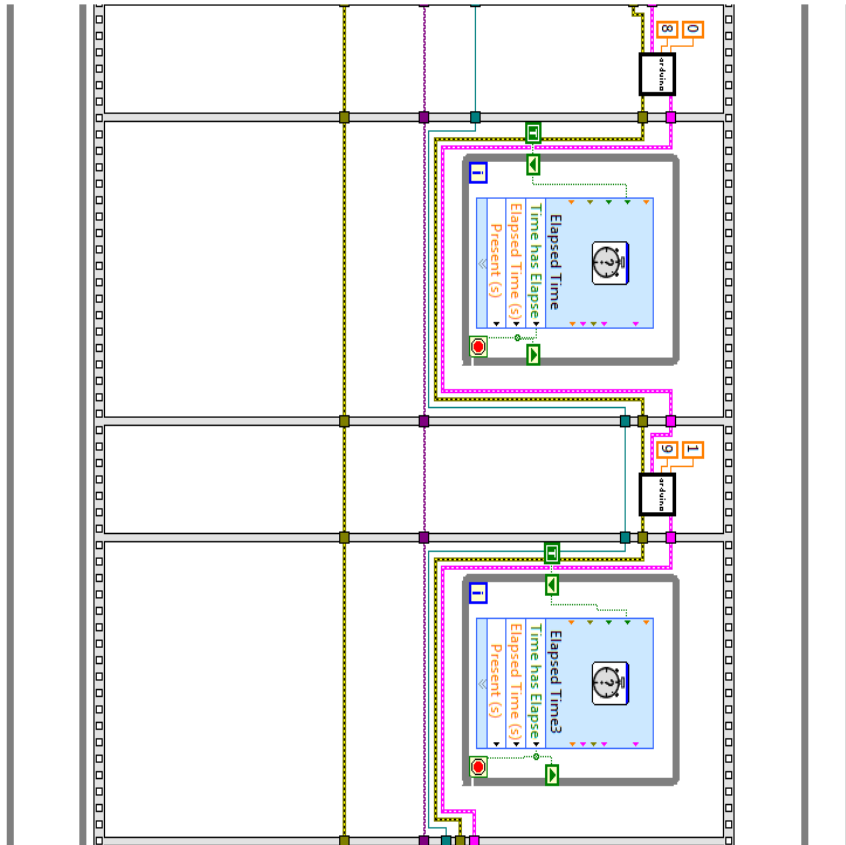
Moreover, an idea for longer-range measuring is needed since at the moment there are only two valve-regulated lead-acid batteries which need to be changed for charging every five days of measuring.

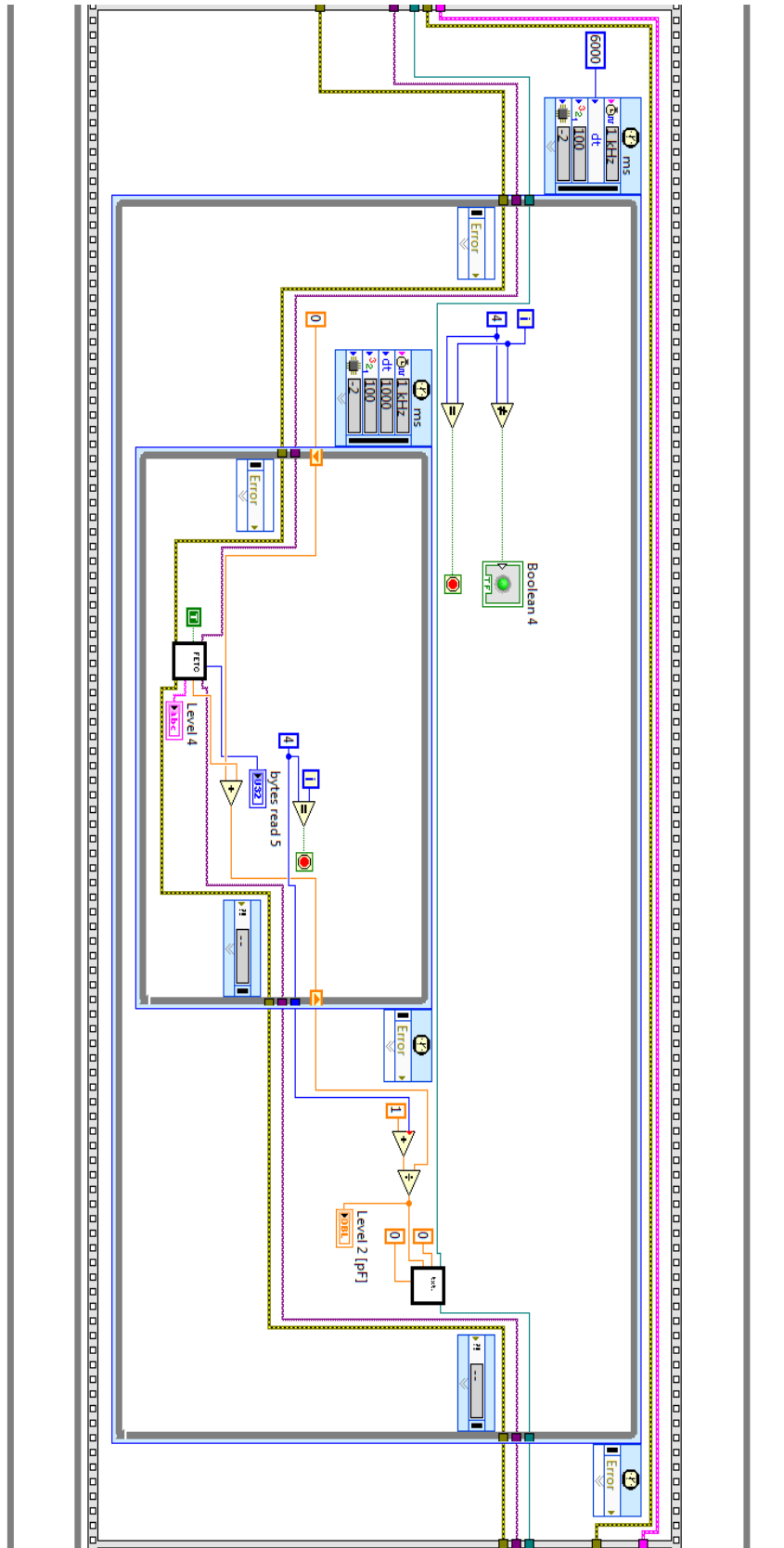
Furthermore a live-display of the liquid level out of the calculation with the calibration would simplify the level monitoring.

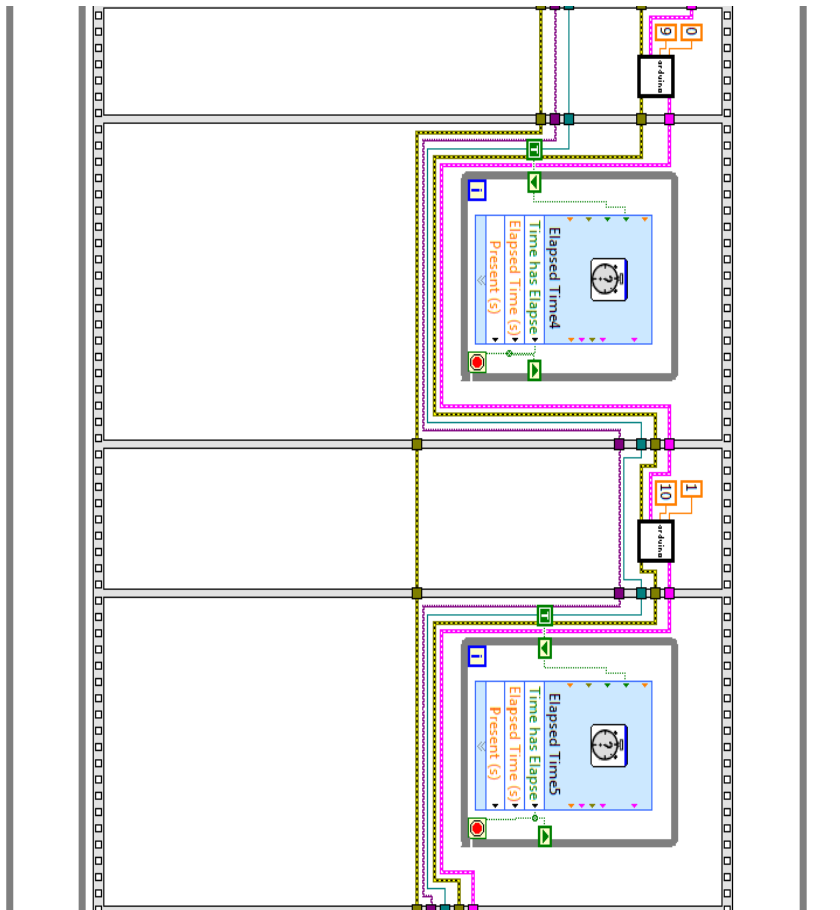
# 6 Appendix

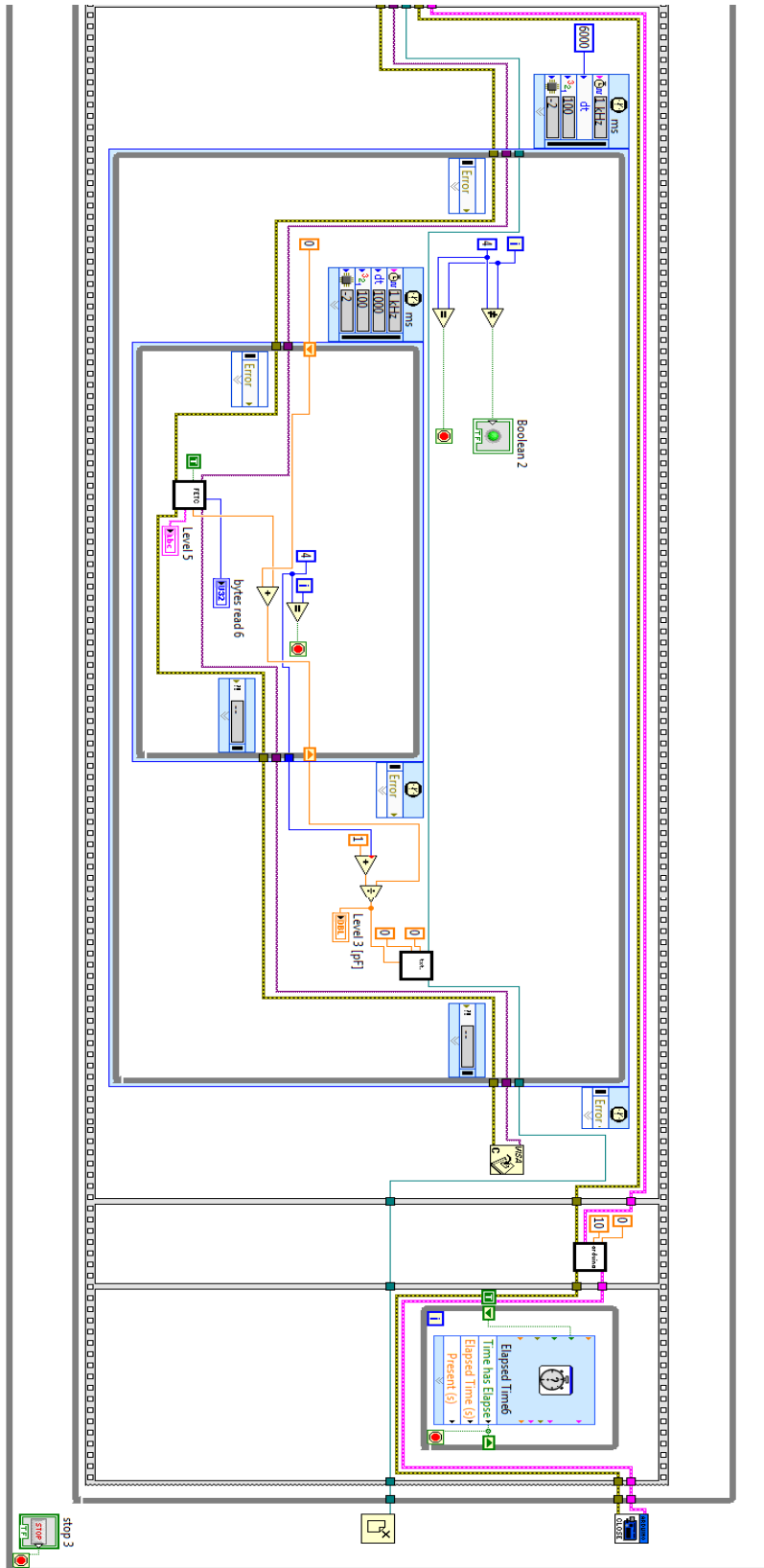


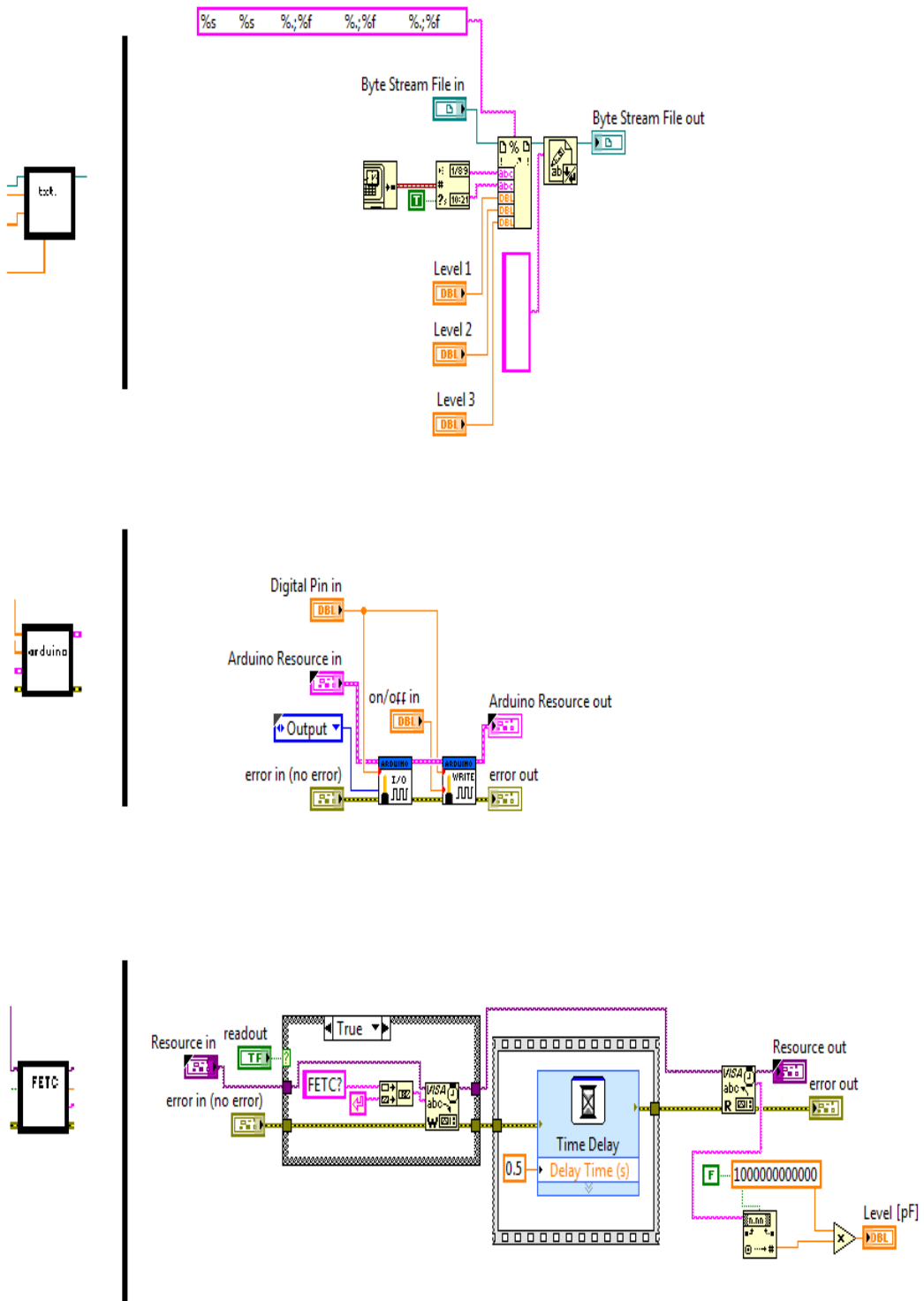












## 7 Bibliography

- [Ang08] J. Angle, et al., "First Results from the XENON10 Dark Matter Experiment at the Gran Sasso National Laboratory", 2008.  
<http://journals.aps.org/prl/abstract/10.1103/PhysRevLett.100.021303>
- [Apr09] E. Aprile and T. Doke, "Liquid Xenon Detectors for Particle Physics and Astrophysics", 2009.  
<http://arxiv.org/pdf/0910.4956.pdf>
- [Apr12a] E. Aprile, et al., "Dark Matter Results from 225 Live Days of XENO100 Data", 2012.  
<http://arxiv.org/pdf/1207.5988.pdf>
- [Apr12b] E. Aprile, et al., "The XENON1T Dark Matter Search Experiment", 2012.  
<http://arxiv.org/pdf/1206.6288.pdf>
- [Apr12c] E. Aprile, et al., "The XENON100 Dark Matter Experiment", 2012.  
<http://arxiv.org/pdf/1107.2155.pdf>
- [Ard16] Arduino, "Arduino UNO & Genuino UNO - Overview", 2016.  
<https://www.arduino.cc/en/Main/ArduinoBoardUno>
- [Bla15] J. Blanke, "Implementation of a Fiberglass Feed-Through into Muenster Time Projection Chamber for the Calibration of Photomultipliers using LED Pulser", bachelor thesis, University of Münster, 2015.
- [Cim13] J. M. Cimbala, "The Gaussian or Normal Probability Density Function", Penn State University, 2013.  
[http://www.mne.psu.edu/cimbala/me345/Lectures/Gaussian\\_or\\_Normal\\_PDF.pdf](http://www.mne.psu.edu/cimbala/me345/Lectures/Gaussian_or_Normal_PDF.pdf)
- [Geo15] W. Georgi et al., "Einführung in LabVIEW", Hanser Fachbuch's 6th ed., 2015.
- [Key14] Keysight Technologies, "Keysight Technologies U1730C Series Handheld LCR Meters", 2014.  
<http://literature.cdn.keysight.com/litweb/pdf/5990-7778EN.pdf>

- [Key15] Keysight Technologies, "Handheld Tools For Electronic, Electrical and Industrial Process Testing", 2015.  
<http://literature.cdn.keysight.com/litweb/pdf/5989-7340EN.pdf>
- [Lid09] D. R. Lide, et al., "Handbook of Chemistry & Physics", Chemical Rubber Company's 90th ed., Boca Raton, 2009.
- [MaB01] M. R. Moldover and T. J. Buckley, "Reference Values of the Dielectric Constant of Natural Gas Components Determined with a Cross Capacitor", 2001.
- [Nat16a] National Instruments, "LabVIEW System Design Software", 2016.  
<http://www.ni.com/labview/>
- [Nat16b] National Instruments, "Data Structures in LabVIEW", 2016.  
<http://www.ni.com/getting-started/labview-basics/data-structures>
- [Tra15] Transtronics Wiki, "Capacitor Codes", 2015.  
[https://wiki.xtronics.com/index.php/Capacitor\\_Codes](https://wiki.xtronics.com/index.php/Capacitor_Codes)

# Declaration of Academic Integrity

I hereby confirm that this thesis on  
**Capacitance-Based Levelmeter Read-Out for the Münster Dual Phase  
Xenon Time Projection Chamber**

is solely my own work and that I have used no sources or aids other than the ones stated. All passages in my thesis for which other sources, including electronic media, have been used, be it direct quotes or content references, have been acknowledged as such and the sources cited.

I agree to have my thesis checked in order to rule out potential similarities with other works and to have my thesis stored in a database for this purpose.

---

*date*

*signature*